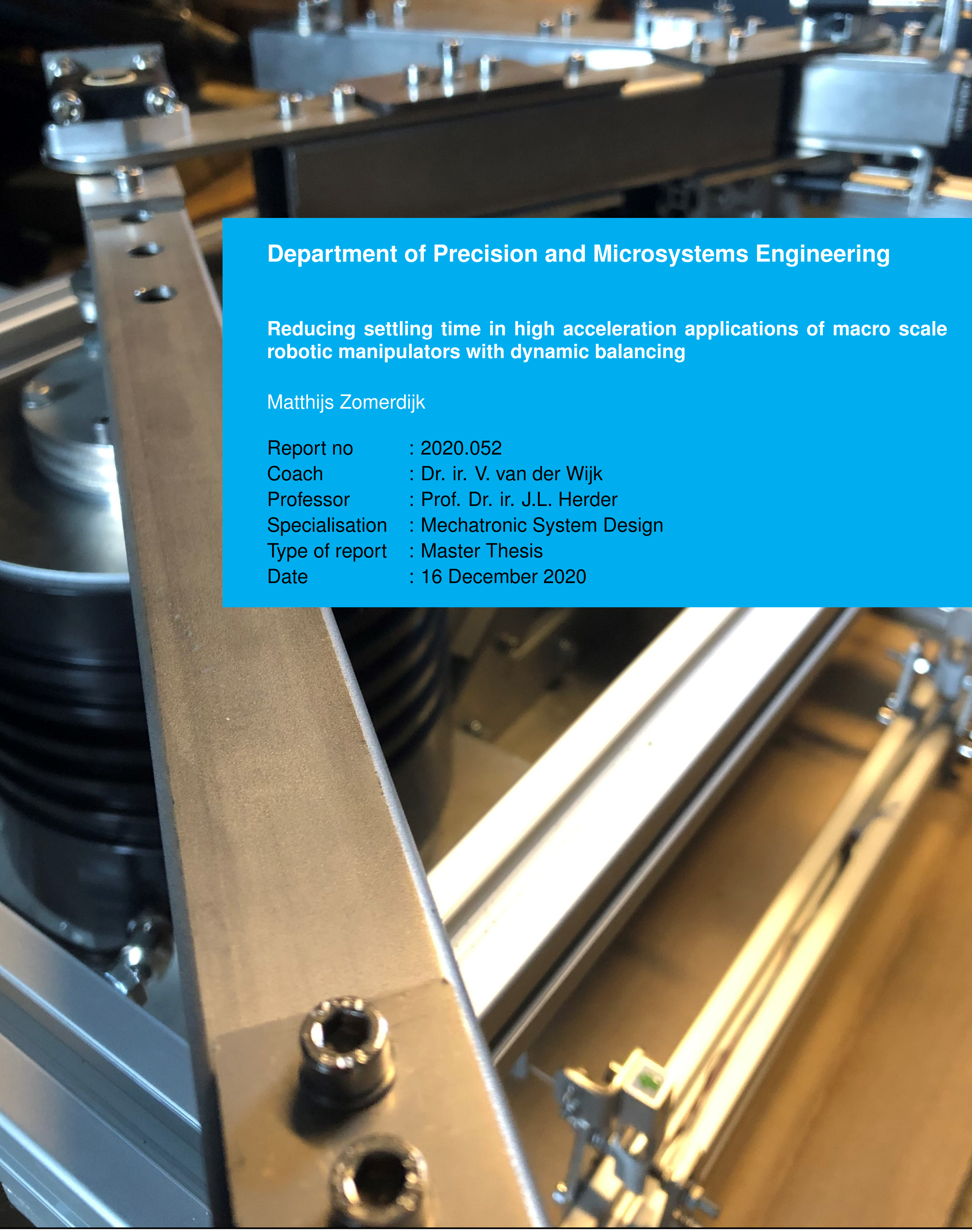

Department of Precision and Microsystems Engineering

Reducing settling time in high acceleration applications of macro scale robotic manipulators with dynamic balancing

Matthijs Zomerdijk

Report no	: 2020.052
Coach	: Dr. ir. V. van der Wijk
Professor	: Prof. Dr. ir. J.L. Herder
Specialisation	: Mechatronic System Design
Type of report	: Master Thesis
Date	: 16 December 2020

Delft University of Technology

Challenge the future

Preface

After more than a year of enjoyable work and dedication, the results of my research are written down in this thesis. The headlines last year were dominated by a particle not larger than 200 nm, which flipped the world upside down. Although a lot of things were not possible, it also resulted in new opportunities. Not only was the concept work from home the new normal, but also research from home, which ultimately resulted into building a prototype and conducting experiments in the garage. But a garage must never be underestimated as an innovative place. Some great inventions, such as the telephone, personal computer, and the pacemaker had their origins in garages.

I would like to thank everyone who helped me during the research and writing of this thesis. In special, my supervisor Volkert van der Wijk for the discussions, many tips and tricks, and reviewing, Jo Spronck for his advise and critical comments which gave food for thought, my colleagues from European Machine Trading (EMT) for sharing their practical knowledge and assistance during manufacturing, and of course my parents for their support and making the garage available.

M.J.J. Zomerdijk
December 2020

Contents

1 Introduction

To stay competitive, in the current ever progressing world, requires to improve performance continuously. In industry, the most relevant purchasing criteria is performance [14]. Performance is in this context the product throughput and accuracy. In pick-and-place applications, the trend to increase throughput is clearly noticeable; the first robotic manipulator in 1961 was designed to achieve 3 cycles per minute [12], while today the Par4 robot reaches 240 cycles per minute [11]. The Par4 robot is designed for packaging applications, but high throughput is also required in semiconductor industry. Common solution to increase throughput, without faster motions, is by picking multiple products at once. Novel applications require additional functionality where the throughput of this solution is limited; for instance sorting, which requires to place products at multiple locations [13]. To move the same amount of products requires in this case a significant larger amount of motions. Achieving an equal throughput therefore requires more cycles per unit time.

The amount of cycles per unit time is determined by the cycle time, which is the time required to complete a single pick-and-place movement. A significant part of the cycle time is determined by the settling time. Settling time is defined as the time to reach and stay within a certain error band of the final position (in this case the pick or place location) after a motion is initiated. Settling time is a combination of motion time and waiting time for vibrations to die out. These vibrations are induced in the manipulator as well as in the base by fluctuating forces and moments exerted by accelerating (and decelerating) elements in the manipulator. Motion time can be reduced by improving acceleration capabilities, while a common solution to reduce the waiting time is by improving controllability and increasing damping. Improving controllability means, in general, increasing the natural frequencies of the mechanism. Increasing damping can be achieved by using materials which have better damping properties or adding actively controlled damping. What is often overlooked is that the waiting time is also influenced by base vibrations. An unbalanced manipulator exerts, due to accelerating (and decelerating) elements in the manipulator, fluctuating reaction forces and reaction moments on base. High acceleration movements of unbalanced manipulators can therefore induce significant base vibrations, which do not only affect the waiting time, but also degenerates precision. In addition, vibrations of one machine can induce vibrations in surrounding machinery attached to the same base or floor. Conventional solutions, such as the addition of force frames and vibration isolation, do not solve the vibrations at the source and may reduce absolute precision.

Dynamic balancing does remove fluctuating reaction forces and reaction moments and therefore eliminates the source of base vibrations. To achieve dynamic balance, the mechanism needs to be both shaking force balanced and shaking moment balanced. The former means no reaction moments are exerted on the base, while the latter means no reaction moments are exerted on the base. Shaking force balance is achieved with the addition of counter-masses, while shaking moment balance is achieved, in general, with the addition of counter-inertias [17]. Distinctive feature of a force balanced mechanism is the stationary centre of mass (CoM) of the complete mechanism, which requires a constant sum of linear momenta during motion. Moment balance is achieved when the sum of angular momenta is constant during motions.

Known experimentally verified high speed dynamically balanced planar manipulators are the DUAL V and Hummingbird manipulator. The DUAL V manipulator relies on actuation redundancy and is based on a duplicate force balanced pantograph architecture [18]. Actuation redundancy means the manipulator has more actuators than degree of freedom (DoF). Accelerations over 10 G are reached with this manipulator during movement (17 cm motion distance). The Hummingbird is a force balanced manipulator with a reaction wheel to achieve dynamic balance [5]. The addition of an actively driven reaction wheel to achieve dynamic balance is also known as active balancing. Accelerations up to 50 G are achieved (5 mm motion distance) with the Hummingbird. Accelerations up to 10 G are reported on a larger scale (25 cm motion distance) with a comparable architecture to the Hummingbird [10, 13].

However, dynamic balancing has, in general, a large drawback: the addition of moving mass and inertia in the mechanism. Natural frequencies are inversely dependent on mass and inertia, therefore additional mass and inertia, in general, degenerates natural frequencies, which reduces controllability and increases the waiting time. Time dependent studies of balanced elastic four-bar mechanisms show an increase in vibrations in the mechanism after balancing [9, 19, 21]. The effect of balancing in the frequency domain is researched for specific cases of a four-bar linkage [7, 8] and a planar force balanced manipulator [1]. In both cases a significant decay in natural frequencies is reported (up to 50%). Despite the reduction in controllability of the mechanism itself, balancing can improve settling time. There are indications that balancing can reduce the settling time by 94% [10, 13].

Research of dynamic balancing in the frequency domain is limited and it is not known which balancing principles result in optimal controllability. In addition, an integral design approach for dynamically balanced mechanisms, which takes controllability into account during the design, is lacking.

1.1. Research objectives

The goal of this thesis is to investigate investigate how settling time of robotic manipulators in a realistic mechatronic environment can be reduced with dynamic balancing. To reach the goal of this thesis three sub-objectives are formulated:

1. Deriving guidelines from literature to determine which aspects help improving settling time in high acceleration applications of robotic manipulators.
2. Comparing existing balancing principles to determine which principles and which configurations have optimal controllability.
3. Presenting and experimentally verifying a design based on a dynamically balanced inverted four-bar linkage with strong potential for high acceleration applications.

While the first goal is applicable to all robotic manipulators, the second and third goal are specifically focussed on balancing,

1.2. Approach and thesis outline

This thesis consists of three papers which correspond with the listed objectives above. The first paper can be regarded as an introduction to the topics settling time and controllability, while the second and third paper are the core of this thesis with the main contributions.

A significant amount of research can be found in literature to reduce settling time and many solutions have been proposed. In the literature study in chapter 2 a set of design principles have been derived from literature which are aimed at reduce settling time in robotic manipulators. These design principles are relevant for robotic manipulators in general, balanced or unbalanced.

Multiple balancing principles are compared in chapter 3 to determine which principle has optimal controllability. Although multiple balancing principles exist, it is not known which principle results in optimal natural frequencies and which parameters need to be optimized to achieve this. Therefore multiple balancing principles are applied to a single rotatable link, which is regarded in this thesis as a building block in manipulator design. The resulting mechanisms are numerically compared to determine which balancing principle has optimal controllability. In addition, the influence of the position of balancing elements on the natural frequencies is investigated.

In Chapter 4 a design is presented and experimentally verified of a balanced rotatable link. Focus of this chapter is on the practical considerations of designing and manufacturing a balanced rotatable link and how to achieve optimal natural frequencies during the design. The architecture of the mechanism is based on the results of chapter 3, therefore the results of chapter 3 form the foundation of chapter 4. In chapter 3 was found that a dynamically balanced inverted four-bar linkage has better controllability than the other balancing principles in the comparison, therefore this architecture is used in chapter 4. After the design, a robustness analysis is conducted to determine the sensitivity to errors during balancing. Finally, the mechanism is built for experimental verification.

Discussion is conducted in chapter 5. In addition, an outlook is given in this chapter how the research could be extended to a multiple degree of freedom (DoF) manipulator.

Finally, conclusions are presented in chapter 6.

2

Design principles to reduce settling time in high acceleration applications of macro scale robotic manipulators

Design principles to reduce settling time in high acceleration applications of macro scale robotic manipulators

M.J.J Zomerdijk, V. van der Wijk

Abstract—**Increasing production requires shorter cycle times of robotic manipulators in high acceleration applications. High acceleration applications are for example pick-and-place applications. A significant part of the cycle time is defined by the settling time, which is the time to reach and stay in a certain error band after a motion is initiated. Settling time can be divided in motion time and waiting time for vibrations to settle (Ts-Tr time). The former depends on the acceleration capabilities of the manipulator, while the latter depends on the controllability. Increasing accelerations to reduce motion time increases vibrations and therefore the Ts-Tr time. This dependency means that the vibrational energy induced by the motion needs to minimized and this minimized energy needs to be dissipated as fast as possible. The goal of this paper is to formulate a set design guidelines aimed at robotic manipulators, that reduce settling time. The design principles are grouped in sub-systems of the complete manipulator. These subsystems are: mechanism, actuation, base, and control. In terms of mechanism topology and geometry a lightweight and stiff manipulator is key. The actuation can be improved by applying actuation redundancy, careful actuator placement, and direct drives. Base vibrations are eliminated by applying dynamic balancing which not only reduce Ts-Tr time, but also improve precision. In terms of control it is important to actuate smooth motions and add feedforward control to reduce abrupt changes in actuation force or torque. Applying these design principles paper will give a firm foundation in the design of robotic manipulators where short settling time is required.**

I. Introduction

In industry, the driving force behind automation is increasing production and improving quality [1]. Increasing production requires shorter cycle times to achieve more cycles per unit time. The Unimate, one of the first robotic manipulators, reached 3 cycles per minute [2], while today the Par4 robot reaches 240 cycles per minute [3]. This is the combined result of increasing accelerations and reducing waiting time in cycles. Improving these two performance indicators results ultimately in a trade-off; higher accelerations reduce motion time, but increase waiting time required for vibrations to settle, this waiting time is defined as the Ts-Tr time (settling time minus rise time). An example of how Ts-Tr time influences settling time is visible in the Hummingbird manipulator. Executing a 5 mm movement with an acceleration of 50 G results in a Ts-Tr time of more than one third of the settling time [4]. At higher accelerations the Ts-Tr time becomes dominant and can even result in longer settling times. Therefore to reduce settling time both motion and Ts-Tr time need to be minimized.

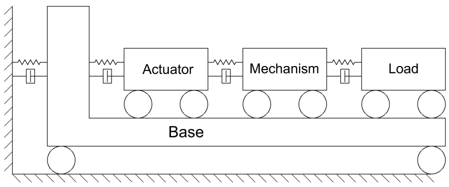

Fig. 1: Simplified physical model of a robotic manipulator. Each body represents a subsystem, assumed is that the base is connected to the fixed world.

The goal of this literature study is to derive a set design principles which reduce settling time in macro scale robotic manipulators. These principles are specifically focussed on high acceleration applications such as pick-and-place and (electric) measuring. In addition to the design principles, this paper also reviews some less conventional approaches to reduce settling time. Therefore this paper can also be used for inspirational purposes, although research opportunities are not explicitly mentioned.

In this literature review the complete manipulator is approached as multiple linear spring-mass-damper subsystems (see Fig. 1). This simplified approach gives a clear overview of the subsystems, but is too coarse for in depth calculations. Each subsystem can be mathematical modelled with linear dynamic Equation 1.

$$M\ddot{x} + C\dot{x} + Kx = F \tag{1}$$

Where M denotes the mass matrix, C the damping matrix, K the stiffness matrix, and F the external applied forces.
This paper is structured according to the subsystems shown in Fig. 1. Section II explains the basics of settling time. In section III the mechanism is reviewed. Section IV focusses on the actuation. In section V, the interaction between the base and the mechanism is studied. Section VI reviews control approaches. Finally, in section VII conclusions are provided. When reading this paper for inspiration, sections III, IV, and V are mainly of interest.

II. Settling time

Settling time is a measure of how fast the system will reach and remain in a certain range of the input value. This range differs from 5% to 1% in literature [5]. The definition of 1%

when applying a step response results in equation 2, for a single spring-mass-damper system.

$$t_s = \frac{4.6}{\zeta\omega_n} \tag{2}$$

Equation 2 shows an inverse relation on the damping ratio and first natural frequency. The former defines how fast vibrations are dissipated, while the latter defines the amplitude of vibrations and the amount of energy stored in vibrations. From an energy perspective, vibrations are an exchange between potential and kinetic energy. Damping dissipates the stored vibrational energy in the system.

Design guideline: A low settling time means reducing the stored amount of vibrational energy and dissipating this minimized energy as fast as possible.

Results of an experimental study reveal that the main sources of vibrations in robotic manipulators are structural elasticity and torque ripples in actuation [6]. Torque ripples occur in many electric motors and cause periodic disturbances in torque. The structural elasticity is a property which is influenced by the stiffness and moving mass of the mechanism. A stiffer design results in a smaller vibration amplitude, while a lower mass means less energy can be stored in vibrations.

Design guideline: Low moving mass reduces the amount of vibrational energy which can be stored in the system.

III. Manipulator

As shown in Fig. 1, the manipulator forms the connection between the actuation and the load. Inverse kinematics and dynamics convert the trajectory of the load to actuation torques or forces. In general a lightweight and stiff mechanism is important to allow fast movements. Reducing settling time by optimal manipulator design is researched in three categories: 1) geometry, 2) topology, and 3) material.

A. Geometry

Geometry defines the locations of links and joints as well as the shape of links. The former is referred to as the manipulator geometry and the latter as link geometry in this study.

Manipulator geometry is predominantly defined by the required workspace, but dexterity, stiffness, payload, and output velocity also have an influence. A larger workspace inevitably results in longer link lengths, which increases mass and degenerates stiffness of the links [7]–[9]. Optimisation of link length when arms are in series, can therefore increase natural frequencies [10], [11]. In case of symmetric five-bar mechanisms (Fig. 2), a performance atlas is available with optimal link ratios [12]. In Fig. 2 is the length of the first link denoted with R1, the second link with R2, and distance between the two base points with R3. High accelerations and low settling time require a mechanism which has a high dexterity and stiffness. Consulting the performance atlas, one of the viable configurations has the ratios $R2 = 2R1$ and $2R2 = 3R3$. These two ratios are a trade-off between dexterity and stiffness. High stiffness requires a wide base combined

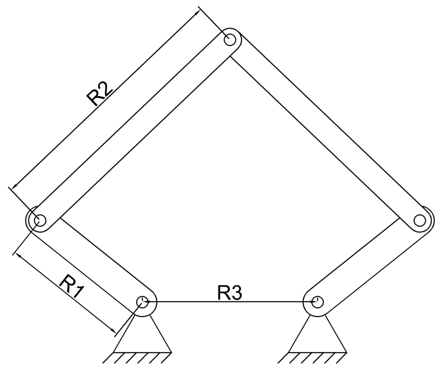

Fig. 2: Five-bar linkage with parameter definitions of link lengths. The link ratios $R2 = 2R1$ and $2R2 = 3R3$, as shown in the figure, results in one of the optimal geometries according to the performance atlas for five-bar linkages in terms of stiffness, workspace, and dexterity [12].

with short first links, while high dexterity is achieved when the first and second link have equal length.

Task specific approaches exchange flexibility for performance, meaning the geometry is altered to the requirements of single trajectories and task spaces. Optimizing the mechanism for these tasks, in terms of cycle time and higher harmonics in the actuation torque, can result in significant performance gain [13]. Frameworks for task specific approaches exist and are used for optimization, but the focus is mainly on the kinematics [14], [15].

Design guideline: Task specific designs have higher performance potential than design which achieve their performance in all conditions.

Link geometries which are optimized for natural frequencies result, in general, in tapered designs of single links [16], [17]. Optimizing stiffness without changing the mass can increase natural frequencies by more than 600 % in comparison to an uniform link [10]. Optimization with the objective to minimize dynamic tip deflection results in designs with optimal settling time [18]. The same research concludes that in cases of fluctuating tip loads, the links need to be optimized for the highest tip load. Links optimized for higher tip loads still perform sufficient at lower loads, while the other way around causes more issues. Minimization of dynamic tip deflection with constraints on mass, static deflection and displacement results in the lowest actuation requirements with an equal cycle time [19]. The same research shows that hollow designs reduce static tip deflection significantly, but require stronger actuators. In multi-link mechanisms the optimal link stiffness depends for a large extent on the kinematic configuration and the choice of actuated joints [20]. In general, the design approach can be applied that links located near the base need to be designed for stiffness. Links located near the load need to be designed for low mass. Links in between require an intermediate approach which depends on the kinematics.

Design guideline: The links closest to the base have the largest influence on the total stiffness, therefore these links require high stiffness. On the other hand, links located near the load need to be designed for low mass.

A significant amount of high speed manipulators have positioned their load at the tip of the manipulator [3], [7], [21]. This seems the most logical position for the load but it may be better to place the load in a node of the most disturbing mode shape. With this approach the load stays stationary when this mode shape is excited. From a different perspective, mode shapes can even be used for energy storage, in flapping-wing micro air-vehicles resonance is used for energy storage and makes the mechanism more efficient [22].

Design guideline: Locating the payload near a node of the most disturbing mode shape reduces the influence of this mode shape on the payload.

B. Topology

The topology of a manipulator defines how the links are arranged with respect to each other. Robotic manipulators can be divided into two basic architectures: 1) serial, and 2) parallel. In parallel architectures, the moving mass is reduced, because all actuators are placed at the base of the manipulator. Parallel topologies also have a higher stiffness due to the closed kinematic loops. While parallel mechanisms are chosen for their high stiffness combined with low moving mass, they also have a few drawbacks: non-constant stiffness, singularities, complex kinematics, and limited workspace [23]. Non-constant stiffness over the workspace of a parallel manipulator can result in position-dependent dynamic responses. Simulations show a 4 degree of freedom (DOF) Delta robot has differing natural frequencies up to 25% [24]. In five-bar planar mechanisms (2 DOF) it can even be up to 50% [25].

Design guideline: Parallel topologies have higher stiffness and lower moving mass compared to serial topologies. Both increase the natural frequencies of the mechanism.

A significant amount of 2 DOF high performance manipulators use parallel mechanisms which are based on six-bar linkages [3], [26]–[28] (Fig. 3a) or degenerated five-bar linkages [7], [29] (Fig. 3b). These two architectures are both based on revolute joints but other joint types are also used. For instance the PRRRP (P-prismatic, R-revolute) configuration is a architecture which combines revolute joints with prismatic joints (shown in Fig. 3c). Compared to a five-bar linkage, the PRRRP configuration has better potential for high velocities but performs worse on accuracy, stiffness, and force transmission [30]. Symmetric spatial manipulators are achieved by adding equal out-of-plane kinematic chains.

Joint type and order of joints have influence on induced vibrations. In a serial topology RR and PR configurations have a higher potential for high harmonic energy transfer than PP types [31]. Disadvantage of a PP configuration is the higher energy demand in actuation, meaning more energy can be transferred to vibrations. Therefore both the ratio of energy transfer and total energy need to be taken into account during design. Additionally each joint without preload can result in backlash and reduces controller performance [32].

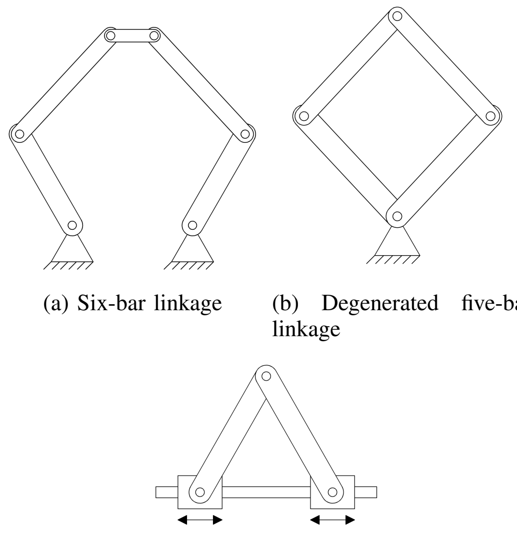

(a) Six-bar linkage (b) Degenerated five-bar linkage

(c) Mechanism with prismatic joints

Fig. 3: Common planar mechanism topologies. Mechanisms which rely only on revolute joints have higher stiffness and accuracy, but potential for high velocities is lower.

A parallel mechanism with prismatic joints can be created in the form of a H-frame, this mechanism is common in 3D printers [33]. Actuation is achieved with belts and motors mounted at the base. The belts are in this setup most critical, due to their elasticity, which also creates differing stiffness throughout the workspace [34].

Adding links which span over the workspace [35] or out-of-plane structures [26] increase stiffness. It needs to be noted that adding complex structures for additional stiffness will not necessary improve natural frequencies due to the added mass [32]. Switching to compliant joints increases, in general, out-of-plane stiffness. Optimizing the orientation of these joints and adding pre-tension even results in stiffer mechanisms with higher natural frequencies [36]. Next to the additional stiffness, compliant joints also remove friction, backlash, and hysteresis in the joints [37]. Attention needs to be paid when using compliant joints that they do not introduce new resonances.

Replacing links with wires will further reduce mass, but requires a completely different design approach because wires can only be loaded in tension. The FALCON manipulator shows that with this concept accelerations up to 43 G are achievable [38]. Main challenge with wire driven manipulators is proper tensioning due to the non-linear behaviour of the cables, which makes modelling and determining stability challenging. Planar wire driven robots have issues with out-of-plane vibrations. Active solutions have been proposed, but result in heavy and complex manipulators [39]. A variation on wire driven robots are spreadbands, which have many similarities with tape measures. They have low friction, no backlash, high repeatability, and a higher stiffness than wires

[40]. The same research suggests accelerations over 100 G are possible, but evidence to support this claim is missing.

Design guideline: Architectures which do not rely on transverse stiffness of links can reduce moving mass in a mechanism.

C. Material

Commonly used material in manipulators is aluminium [7], [41], because of low material cost, low mass, and good machinability. The links located near the load (distal links) can also be made from magnesium [21]. This material has lower density and better damping properties than aluminium [42]. Composing links out of multiple materials along the length of the link can increase performance [43]. Heavier and stiffer material is located near the base, while lighter and more elastic material is located at the tip. Main challenge is to join these materials seamlessly. Additional damping can be achieved with coatings [44] and sandwich structures [45]. Last few years composite materials have become more common due to their low mass and high stiffness [3], [24], [26]. Additional damping in composites can be created by adding visco-elastic layers [46]. A remark must be made that higher damping also reduces the efficiency of the mechanism, it could therefore be advantageous to use active switchable damping.

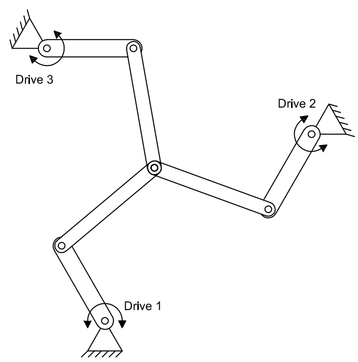

Fig. 4: Parallel mechanism with permanent actuation redundancy. The mechanism is 2 DoF with 3 drives, which means 1 drive is redundant

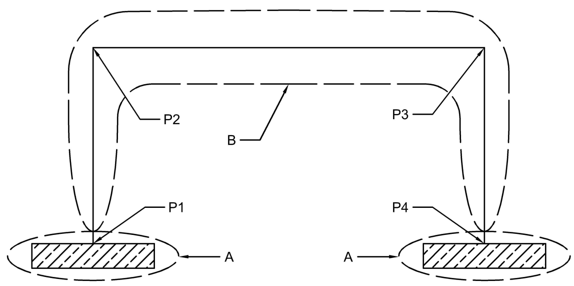

Fig. 5: Pick-and-place motion. Picking and placing occurs in the areas indicated with an A, bulk motion is executed in area B. The motion picks the object in point P1, moves trough P2 and P3, and places in point P4. High accuracy is beneficial in area A, high accelerations and velocities are beneficial in area B.

IV. Actuation

The actuators convert electric signals generated by the controller to a force or torque. Actuation can be both linear as rotational whereas this depends on the architecture of the mechanism.

A. Actuation redundancy

Actuation redundancy is created by adding more actuators than DOF (Fig. 4), which improves acceleration capabilities, dynamics [47], and stiffness [48], [49]. This approach is used in multiple manipulators [35], [38], [50], the NINJA manipulator even uses 8 drives for 6 DOF. While these robots use a permanent drive configuration it is also possible to implement redundancy in a reconfigurable way. This concept is called virtual force redundancy (VFR) [51]. In VFR the motion is divided into a bulk motion, which requires high accelerations, and a fine motion, which has additional DOF or improved accuracy. A pick-and-place task is shown in Fig. 5. The motion starts in point P1 goes through P2 and P3 and ends in P4. Precise movements are required in area A (picking or placing) and bulk motion (movement) is executed in area B. VFR is created by adding a differential mechanism to the actuators. When the actuators move in the same direction VFR is activated. If they move in opposite directions additional DOF or accuracy is added. The complexity of this mechanism is also the main drawback. When linear actuators are used a differential mechanism is not necessary; this can be seen in the Arrow V1 robot which has actuation redundancy for movements on the X-axis [52]. In fact every manipulator which is based on a PRRRP configuration has this property [48], [53]. The concept of VFR is also applicable in wire driven robots; with the help of additional pulleys accuracy is improved when needed [54]. Actuation redundancy creates an overconstrained system which can result in high internal forces. When controlled properly, these forces are not necessary a disadvantage and can be used to control the mechanism stiffness actively [55].

Design guideline: Actuation redundancy by adding more actuators than DOF increases stiffness and acceleration capabilities.

B. Actuation application point

The base of a link is often where actuation is applied but this is not necessary the optimal location. By optimizing the application point the cycle time of a manipulator can be reduced up to 50% [11]. Combining actuation in nodes with actuation redundancy has yielded significant improvements in wafer chucks. The chuck was designed in such a way that the nodes of the first five mode shapes are in the same location, resulting in a lightweight chuck with a double control bandwidth compared to a non-optimized design [56]. The concept is explained by applying it to a simply supported beam which can move up and down, rollers at both sides prevent the beam from tilting. Actuation is provided by force F. In conventional cases actuation is located at the centre of the beam (see Fig. 6a). Placing the actuation point in a node of a mode shape prevents excitation, this can be seen in Fig. 6b. Drawback of this approach is that the mode becomes uncontrollable. Removing excitation of modes is beneficial for feedforward control but feedback control requires controllability of the mode for optimal performance. To prevent excitation combined with controllability requires an additional actuator in an anti-node (See Fig. 6c). With this approach actuation redundancy is created and the frequency of the first parasitic resonance peak almost triples [57]. The same results can be achieved with symmetric actuation in anti-nodes (See Fig. 6d). Attention should be paid to the influence of changing payloads on the mode shapes. Out-of-plane mode shapes can be reduced by placing actuation torques and the centre of mass (CoM) of moving elements in the same plane. The removal of out-of-plane torques results in significantly less excitation of out-of-plane mode shapes [58].

Design guideline: Feedback control performance is improved when actuation is applied in an anti-node of a mode shape, making the mode shape controllable.

Design guideline: Feedforward control performance is improved when actuation is applied in a node of a mode shape, preventing excitation of the mode shape.

When endpoint control is implemented to improve accuracy, the system becomes non-collocated, which results in a non-minimum phase behaviour and limited controller bandwidth [59]. To create a completely collocated system can be challenging, but by moving the sensor and actuator closer to each other the influence of non-collocation shifts to higher frequencies [60]. In case of a rotary actuator, collocation can be achieved by mounting the sensor at the shaft of the actuator. Caution is required to maintain observability of important mode shapes.

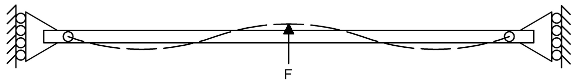

(a) Conventional actuation (mode shape excited and controllable)

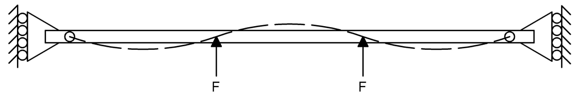

(b) Nodal actuation (mode shape not excited and not controllable)

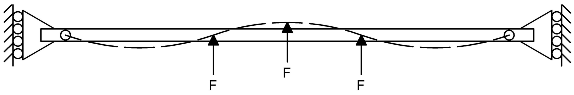

(c) Redundant symmetric actuation (mode shape controllable and not excited)

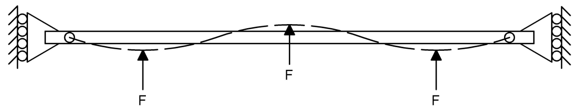

(d) Redundant symmetric actuation in anti-nodes (mode shape controllable and not excited)

Fig. 6: Actuation points in a simply supported beams taking mode shapes into account. Feedback control performance is improved when actuation is applied in an anti-node (Fig. 6a). Feedforward control performance is improved when actuation is applied in nodes (Fig. 6b).

C. *Micro-macro actuation*

In micro-macro setups the motion is divided in a bulk and precise motion in the same way as VFR, therefore Fig. 5 is applicable. In area A the micro stage increases accuracy, while in area B the macro stage increases speed and acceleration. Micro-macro stages are commonly used in hard disk drives [61] and precise high speed motion stages [62]–[64]. To decrease cycle times, the micro stage can perform a combined function as anti-vibration system and fine motion stage. In anti-vibration mode vibration amplitudes are reduced to the maximum stroke of the micro stage. Successively accurate positioning is initiated [65]. Experiments show reductions of more than 30 % in waiting time before precise positioning can start.

Design guideline: When micro-macro actuation is applied, the micro stage, which has often an higher control bandwidth than the macro stage, can be used to attenuate vibrations in the macro stage.

D. *Piezoelectric damping*

Vibration suppression is achieved by placing piezoelectric transducers (PZT) on the links. Most effective is to place the PZT in anti-nodes of mode shapes. These locations have the highest modal strain energy [66]. Approaches can be both passive or active. In passive setups the PZT is shunted with a resistor and activated when vibration suppression is required [67]. With passive setups, material loss factors have been achieved up to 42 % in longitudinal vibrations and 8 % in transverse vibrations. In comparison, aluminium has only a loss factor of 0.1 % in transverse cases [68]. Damping in a passive PZT setup is frequency dependent due to the resistor and capacitance of the PZT creating a RC circuit. Main advantage of passive PZT damping over viscoelastic materials is the higher total structural damping per unit mass. Equal behaviour can be created with an eddy current damper [69]. Active PZT damping results in higher performance, but also increases complexity. Addition of active PZT to the PAR2 robot reduced the cycle time with 63 % [70].

Design guideline: Passive PZT damping is more efficient than adding visco elastic materials in terms of stiffness to weight ratio, resort to active PZT damping if the manipulator does not have the required performance.

E. Drives

Direct drives are the preferred type of actuation for high speed manipulators. These drives have no backlash and limited friction [71], on top of that no transmission is needed which reduces inertia and improves dynamics [47]. Main problem in drives are torque ripples which can induce serious vibrations [6]. These ripples are a result of switching magnetic fields inside the motor. Determining during the design process which drive produces minimal torque ripples is difficult. A high number of slots and poles inside the motor gives an indication of a low torque ripple, although much more factors are of influence [72].

Design guideline: The usage of direct drives results in higher performance, attention needs to be paid to torque ripples.

V. Base

Assumed in this paper is that base connected to the fixed world. The base forms with this definition the connection between the manipulator and the fixed world. Vibrations in the base would therefore affect position accuracy and increase settling time. Additionally, vibrations will be induced on other machinery and measurement equipment, requiring force frames and vibration isolation.

A. Properties of the base

Base vibrations are a consequence of compliance between the base and the fixed world. Fluctuating reaction forces and reaction moments exerted on the base by the mechanism will therefore result in base vibrations. Increasing stiffness of the base is challenging, therefore mass and damping should be increased to reduce the amplitude of vibrations. A higher mass means more energy is required to induce the same vibration amplitude. By choosing a material which has higher damping, for example epoxy-granite [73], more vibrational energy is dissipated. These two improvements are more convenient to implement in large stationary machines than in small mobile machines.

B. Balancing

Removing fluctuating reaction forces and moments exerted on the base altogether requires a manipulator which is dynamically balanced. Dynamic balance means the sum of all linear and angular momenta stays constant during all motions, resulting in a stationary CoM. A force balanced solution means the manipulator does not exert any fluctuating forces on the base. A moment balanced solution does not exert any fluctuating moments [74].

Dynamical balanced mechanisms based on a force balanced five-bar linkage with a reaction wheel (Fig. 7) are already introduced in industry [7], [29]. The mechanism show a significant reduction in settling time [75]. Research over the years generated more sophisticated designs with less mass and inertia [76], [77]. Multiple principles exist to achieve a dynamically balanced mechanism [41]. Main problem with balancing, in general, is the addition of mass in the mechanism, which degenerates natural frequencies of the mechanism.

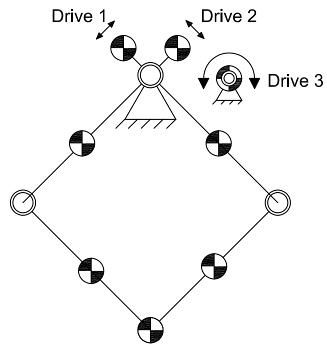

Fig. 7: Dynamically balanced manipulator based on a force balanced five-bar linkage with a reaction wheel.

Active balancing, with counter moving mechanisms [78], results in more flexibility and robustness against payload fluctuations. Disadvantage of a active solution is the increased complexity due to additional actuators and control. Additionally, sometimes such fine motions are required that the control system is not sufficient [4]. Partial balanced solutions show advantages in terms of frequency response [79] and accuracy [80]. The performance of partial balancing will depend on the properties of the base, results are therefore case specific.

Balancing without altering the mechanism can be achieved by generating partial balanced paths. For a 5-bar planar mechanism this approach results in a reduction of shaking forces up to 32% [81].

Design guideline: Balancing reduces base vibrations which improves absolute precision and settling time of the manipulator. Attention needs to be paid to the increased moving mass which reduces controllability.

VI. Motion control

Motion control translates a task into electric signals for the actuators. In general a motion controller can be split into four subtasks [82]: 1) trajectory planning, 2) profile generation, 3) feedforward control, and 4) feedback control. This section will be arranged according to these subtasks.

A. Trajectory planning

Trajectory planning navigates the manipulator through the workspace. A square trajectory is shown in Fig. 5. Main problem with such a trajectory are the straight angles at the corner points (points P2 and P3). Straight angles require first to accelerate and decelerate in one direction and successively in the other. Using a curved path means acceleration and deceleration of multiple axis can occur simultaneously, reducing path jerk [83].

To reduce base vibrations it is beneficial to generate trajectories which are balanced. Even when a mechanism is not dynamically balanced it is still possible to move minimal reactions [35], [84].

Design guideline: Smooth and balanced trajectories avoids vibrations. Applying a fillet to a straight corner results in a much smoother trajectory.

B. Profile generation

Profile generation converts trajectories to accelerations and velocities. Higher-order motion profiles induce less vibrations than trapezoidal motion profiles because of their finite jerk [83], [85], [86] and much lower spectral content [87]. An even smoother motion profile can be created by using sinusoidal shaped jerk profiles [88].

Another technique is input shaping. This method works with timing multiple impulses which counter the vibrations induced by the previous impulse, reducing vibrations up to 25 times [89]. Additional derivatives in zero vibration (ZV) input shapers increase robustness due to additional damping, but also increase motion time [90].

Design guideline: Smooth motion profiles avoids vibrations due to finite jerk, which means that accelerations and forces are built up fluently.

C. Feedback control

The goal of feedback control is to minimize the error between reference and plant output. Feedback control can only react if there is an error and therefore adjustments are reactive. In the feedback control design a trade-off has to be made between bandwidth, range, and precision [91]. A higher bandwidth decreases precision due to higher sensor frequencies with more noise. A larger range means lower natural frequencies which decreases bandwidth. A larger range will also result in quantization errors and reduced precision. This trade-off therefore means an optimum needs to be found between these three parameters.

Design guideline: Mechanisms with high natural frequencies have lower a settling time due to higher control bandwidths.

PID control is a common used feedback control technique due to its simplicity and acceptable performance [59]. In terms of settling time it may be beneficial to use PD control because of the higher damping, but this type of control will have a steady state error and is more sensitive to noise. To increase bandwidth resonance peaks can be cancelled with a notch filter [92], drawback of this approach is the lack of robustness. H_∞ control is more sophisticated than PID and takes resonances into account. Next to higher robustness, H_∞ control also reaches higher closed loop bandwidths [93].

Variable-structure control (VSC) has the ability to switch between multiple controllers with multiple objectives such as vibration suppression, disturbance rejection, accuracy, and robustness [32]. VSC can be divided into sliding mode and soft VSC. Sliding mode creates discontinuities in control signals, while soft VSC has continuous control signals. The continuous signals are achieved because soft VSC has an infinite amount of sub-controllers.

D. Feedforward control

With feedforward control a better match between system and controller is achieved which reduces vibrational energy [94]. Feedforward control can be divide into two approaches: model and data based. Model based control relies on a inverse model of the system while data based approaches learn from measurements.

In model based approaches it is important that an accurate model is available otherwise unmodeled dynamics and simplifications will deteriorate performance [95]. Unmodeled dynamics can be solved in two ways: 1) designing a manipulator which is less complex to model or 2) making a more detailed model. Attention needs to be paid to crosstalk between dynamic subsystems caused by cables or hoses [96]. Feedforward is often combined with feedback to compensate for factors as non-linear damping, unmodeled dynamics and disturbances [82]. By reducing the amount of unmodeled dynamics, feedback control can be tuned for disturbance rejection, with better performance as result. Combining feedforward with feedback control and input shaping can reduce time with a factor two when compared to feedback control only [90]. A different form of errors are manufacturing tolerances, which can be resolved with calibration.

Design guideline: Feedforward limits vibrational energy in the system. Performance is increased by more sophisticated models.

Data based feedforward control does not use models to calculate the motions but uses measured information from the system. Iterative learning control (ILC) uses sensor data to compare the planned trajectory with the measured trajectory and adjusts the controller that these two match [59]. Disadvantage of this type of control is the poor performance at non-repetitive trajectories. By applying segmented ILC the task will be divided into multiple subtasks which reduces this problem [97]. Novel research is aimed to combine ILC with parametrized feedforward control to create a controller which has high performance in both repetitive and non-repetitive tasks [98].

E. Sensors

A sensor is necessary for feedback control to determine the error of the system. The position of a sensor influences the observability of the system; when a sensor is placed in a node of a mode shape the sensor will not measure any displacement. By optimizing the position of the sensors settling time will be reduced [99]. At higher control bandwidths sensors can generate noise which affects feedback control negatively. While it is impossible to remove all noise from measurements, reducing it by proper shielding and digitalizing the signal as soon as possible is recommended.

Design guideline: Reducing sensor noise improves feedback control.

VII. Conclusion

This literature review had the goal to derive design principles to reduce settling time in macro scale robotic manipulators. The amount of design principles reveals that settling depends on many variables. The approaches to reduce settling time are therefore nearly limitless, which also means the approaches in this paper are only a selection of most common and innovative approaches. Main line to reduce settling time is to increase natural frequencies and damping, additionally it is important to eliminate sources of vibration. Natural frequencies define which vibrations are induced on the manipulator and how much energy can be stored. Damping defines how fast vibrations can be dissipated. The manipulator was divided into multiple subsystems and design principles were grouped according to these subsystems. These subsystems are: mechanism, actuation, base, and control. Mechanism design of manipulators requires optimal mass to stiffness ratios combined with optimized link lengths in kinematic chains. In terms of mechanism topology and geometry a lightweight and stiff mechanism is key. The actuation can be improved by applying actuation redundancy, careful actuator placement, and direct drives. Base vibrations are eliminated by applying dynamic balancing which not only reduce Ts-Tr time, but also improve precision. In terms of control it is important to actuate smooth motions and add feedforward control to reduce abrupt changes in actuation force or torque. Additional damping to increase dissipation of vibrations can be achieved passively and actively. Main advantage is that passive damping does not rely on control. Passive damping can be achieved with materials which have good damping properties and visco-elastic layers. Active damping is commonly achieved with piezoelectric elements and often outperforms passive damping. Applying the design principles formulated in this paper will give a firm foundation in the design of robotic manipulators where short settling time is required.

References

[1] M. Teulieres, J. Tilley, L. Bolz, P. M. Ludwig-Dehm, and S. Wägner, "Industrial robotics: Insights into the sector's future growth dynamics," Jul 2019. [Online]. Available: https://www.mckinsey.com/~/media/McKinsey/Industries/AdvancedElectronics/OurInsights/Growthdynamicsinindustrialrobotics/Industrial-robotics-Insights-into-the-sectors-future-growth-dynamics.ashx

[2] S. Y. Nof, *Handbook of industrial robotics*. Wiley, 1999.

[3] V. Nabat, M. de la O Rodriguez, O. Company, S. Krut, and F. Pierrot, "Par4: very high speed parallel robot for pick-and-place," in *2005 IEEE/RSJ International Conference on Intelligent Robots and Systems*. IEEE, 2005, pp. 553–558.

[4] L. C. Zai, L. F. Durfee, D. G. Manzer, J. P. Karadis, M. P. Mastro, and L. W. Landerman, "Control of a hummingbird minipositioner with a multi-transputer MARC controller," pp. 534–541, 1992.

[5] G. F. Franklin, J. D. Powell, and A. Emami-Naeini, *Feedback control of dynamic systems*. Pearson, 2015.

[6] G. Ferretti, G. Magnani, and P. Rocco, "Force oscillations in contact motion of industrial robots: An experimental investigation," *IEEE/ASME Transactions on Mechatronics*, vol. 4, no. 1, pp. 86–91, 1999.

[7] J. Karidis, G. McVicker, J. Pawletko, L. Zai, M. Goldowsky, R. Brown, and R. Comulada, "The Hummingbird minipositioner-providing three-axis motion at 50 g's with low reactions," in *Proceedings 1992 IEEE International Conference on Robotics and Automation*, vol. 1. IEEE Comput. Soc. Press, 1992, pp. 685–692.

[8] C. Park, D. I. Park, H. M. Do, and B. I. Kim, "Structural analysis of a high speed parallel manipulator," *2013 10th International Conference on Ubiquitous Robots and Ambient Intelligence, URAI 2013*, pp. 178–181, 2013.

[9] Y. K. Yong, S. O. Moheimani, B. J. Kenton, and K. K. Leang, "Invited review article: High-speed flexure-guided nanopositioning: Mechanical design and control issues," *Review of Scientific Instruments*, vol. 83, no. 12, 2012.

[10] F.-Y. Wang, Y. Gao, J. L. Russell, and Y. Gao, "Optimum Shape Design of Flexible Manipulators with Tip Loads," *Advanced Studies of Flexible Robotic Manipulators*, pp. 319–362, 2003.

[11] J. H. Park and H. Asada, "Concurrent design optimization of mechanical structure and control for high speed robots," *Journal of Dynamic Systems, Measurement and Control, Transactions of the ASME*, vol. 116, no. 3, pp. 344–356, 1994.

[12] X. J. Liu, J. Wang, and G. Pritschow, "Performance atlases and optimum design of planar 5R symmetrical parallel mechanisms," *Mechanism and Machine Theory*, vol. 41, no. 2, pp. 119–144, 2006.

[13] J. S. Rastegar, L. Liu, and D. Yin, "Task-specific optimal simultaneous kinematic, dynamic, and control design of high-performance robotic systems," *IEEE/ASME Transactions on Mechatronics*, vol. 4, no. 4, pp. 387–395, 1999.

[14] S. Patel and T. Sobh, "Task based synthesis of serial manipulators," *Journal of Advanced Research*, vol. 6, no. 3, pp. 479–492, 2015.

[15] J. Y. Kim, "Task based kinematic design of a two DOF manipulator with a parallelogram five-bar link mechanism," *Mechatronics*, vol. 16, no. 6, pp. 323–329, 2006.

[16] F. Y. Wang, "Optimum design of vibrating cantilevers: A classical probem revisited," *Journal of Optimization Theory and Applications*, vol. 84, no. 3, pp. 635–652, 1995.

[17] B. L. Karihaloo and F. I. Niordson, "Optimum design of vibrating cantilevers," *Journal of Optimization Theory and Applications*, vol. 11, no. 6, pp. 638–654, 1973.

[18] S. Mahto, "Shape optimization of revolute-jointed single link flexible manipulator for vibration suppression," *Mechanism and Machine Theory*, vol. 75, pp. 150–160, 2014.

[19] U. S. Dixit, R. Kumar, and S. K. Dwivedy, "Shape optimization of flexible robotic manipulators," *Journal of Mechanical Design, Transactions of the ASME*, vol. 128, no. 3, pp. 559–565, 2006.

[20] B. Lim and F. C. Park, "Minimum vibration mechanism design via convex programming," *Journal of Mechanical Design, Transactions of the ASME*, vol. 131, no. 1, pp. 0 110 091–0 110 099, 2009.

[21] K. Nagai, M. Matsumoto, K. Kimura, and B. Masuhara, "Development of parallel manipulator "NINJA" with ultra-high-acceleration," in *2003 IEEE International Conference on Robotics and Automation (Cat. No.03CH37422)*, vol. 3. IEEE, 2003, pp. 3678–3685.

[22] S. S. Baek, K. Y. Ma, and R. S. Fearing, "Efficient resonant drive of flapping-wing robots," *2009 IEEE/RSJ International Conference on Intelligent Robots and Systems, IROS 2009*, pp. 2854–2860, 2009.

[23] J.-P. Merlet and C. Gosselin, "Parallel Mechanisms and Robots," *Springer Handbook of Robotics*, pp. 269–285, 2008.

[24] Y. Li, Y. Ma, S. Liu, Z. Luo, J. Mei, T. Huang, and D. Chetwynd, "Integrated design of a 4-DOF high-speed pick-and-place parallel robot," *CIRP Annals*, vol. 63, no. 1, pp. 185–188, 2014.

[25] J. Tlusty, J. Ziegert, and S. Ridgeway, "Fundamental Comparison of the Use of Serial and Parallel Kinematics for Machines Tools," *CIRP Annals*, vol. 48, no. 1, pp. 351–356, jan 1999.

[26] F. Pierrot, C. Baradat, V. Nabat, O. Company, S. Krut, and M. Gouttefarde, "Above 40g acceleration for pick-and-place with a new 2-dof PKM," *Proceedings - IEEE International Conference on Robotics and Automation*, vol. 2, pp. 1794–1800, 2009.

[27] T. Huang, Z. Li, M. Li, D. G. Chetwynd, and C. M. Gosselin, "Conceptual design and dimensional synthesis of a novel 2-DOF translational parallel robot for pick-and-place operations," *Journal of Mechanical Design, Transactions of the ASME*, vol. 126, no. 3, pp. 449–455, 2004.

[28] T. Akima, "Hybrid Micro-Gravity Simulator Consisting of a High-speed Parallel Robot," *October*, no. May, pp. 2–7, 2004.

[29] H. F. Menschaar, A. B. Ariens, J. L. Herder, and B. M. Bakker, "Five-bar mechanism with dynamic balancing means and method for dynamically balancing a five-bar mechanism," WIPO Patent WO2 006 080 846A1, 2006.

[30] S. Sun, J. W. Cheung, and Y. Lou, "A study on five-bar manipulators for semiconductor packaging applications," *Proceedings of the 2007 IEEE*

International Conference on Mechatronics and Automation, ICMA 2007, pp. 1811–1816, 2007.
[31] Q. Tu and J. Rastegar, "The effects of the manipulator type on the vibrational excitation during motion," *Mechanism and Machine Theory*, vol. 32, no. 2, pp. 221–233, feb 1997.
[32] H. Ding and Z. Xiong, "Motion stages for electronic packaging design and control," *IEEE Robotics and Automation Magazine*, vol. 13, no. 4, pp. 51–61, 2006.
[33] I. E. Moyer, "Principle of operation, corexy mechanism," 2012. [Online]. Available: https://corexy.com/theory.html
[34] K. Sollmann, M. Jouaneh, and D. Lavender, "Dynamic Modeling of a Two-Axis, Parallel, H-Frame-Type XY Positioning System," *IEEE/ASME Transactions on Mechatronics*, vol. 15, no. 2, pp. 280–290, 2010.
[35] V. van der Wijk, S. Krut, F. Pierrot, and J. L. Herder, "Design and experimental evaluation of a dynamically balanced redundant planar 4-RRR parallel manipulator," *The International Journal of Robotics Research*, vol. 32, no. 6, pp. 744–759, 2013.
[36] R. Cornelissen, A. Müller, and R. Aarts, "A Compliant and Redundantly Actuated 2-DOF 3RRR PKM: Best of Both Worlds?" in *Computational Methods in Applied Sciences*. Springer, 2020, vol. 1, pp. 163–171.
[37] L. L. Howell, *Compliant mechanisms*. John Wiley & Sons, 2002.
[38] S. Kawamura, W. Choe, S. Tanaka, and H. Kino, "Development of an Ultrahigh Speed Robot FALCON Using Parallel Wire Drive Systems." *Journal of the Robotics Society of Japan*, vol. 15, no. 1, pp. 82–89, 1997.
[39] R. De Rijk, M. Rushton, and A. Khajepour, "Out-of-Plane Vibration Control of a Planar Cable-Driven Parallel Robot," *IEEE/ASME Transactions on Mechatronics*, vol. 23, no. 4, pp. 1684–1692, 2018.
[40] H. A. Schmid, "Spreadbands drive parallel robots," *Industrial Robot*, vol. 28, no. 4, pp. 320–327, 2001.
[41] V. van der Wijk, J. L. Herder, and B. Demeulenaere, "Comparison of various dynamic balancing principles regarding additional mass and additional inertia," *Journal of Mechanisms and Robotics*, vol. 1, no. 4, pp. 1–9, 2009.
[42] J. Zhang, R. J. Perez, and E. J. Lavernia, "Documentation of damping capacity of metallic, ceramic and metal-matrix composite materials," *Journal of Materials Science*, vol. 28, no. 9, pp. 2395–2404, 1993.
[43] Y. S. Liao, "A Generalized Method For The Optimal Design Of Beams Under Flexural Vibration," *Journal of Sound and Vibration*, vol. 167, no. 2, pp. 193–202, 1993.
[44] H. Y. Yen and M. H. Herman Shen, "Passive vibration suppression of beams and blades using magnetomechanical coating," *Journal of Sound and Vibration*, vol. 245, no. 4, pp. 701–714, 2001.
[45] E. El-Dannanh and S. Farghaly, "Vibratory response of a sandwich link in a high speed mechanism," *Mechanism and Machine Theory*, vol. 28, no. 3, pp. 447–457, may 1993.
[46] R. F. Gibson, "Damping characteristics of composite materials and structures," *Journal of Materials Engineering and Performance*, vol. 1, no. 1, pp. 11–20, 1992.
[47] D. Corbel, M. Gouttefarde, O. Company, and F. Pierrot, "Towards 100G with PKM. Is actuation redundancy a good solution for pick-and-place?" *Proceedings - IEEE International Conference on Robotics and Automation*, no. section IV, pp. 4675–4682, 2010.
[48] J. Wu, X. Chen, T. Li, and L. Wang, "Optimal design of a 2-DOF parallel manipulator with actuation redundancy considering kinematics and natural frequency," *Robotics and Computer-Integrated Manufacturing*, vol. 29, no. 1, pp. 80–85, feb 2013.
[49] H. Sadjadian and H. D. Taghirad, "Kinematic, singularity and stiffness analysis of the hydraulic shoulder: A 3-d.o.f. redundant parallel manipulator," *Advanced Robotics*, vol. 20, no. 7, pp. 763–781, 2006.
[50] G. S. Natal, A. Chemori, and F. Pierrot, "Dual-space control of extremely fast parallel manipulators: Payload changes and the 100G experiment," *IEEE Transactions on Control Systems Technology*, vol. 23, no. 4, pp. 1520–1535, 2015.
[51] K. Nagai, Y. Nishibu, Y. Dake, and A. Yamanaka, "Design of a high speed parallel mechanism based on Virtual Force Redundancy concept," in *2009 IEEE International Conference on Industrial Technology*, vol. 2. IEEE, feb 2009, pp. 1–6.
[52] S. Shayya, S. Krut, O. Company, C. Baradat, and F. Pierrot, "Dimensional synthesis of 4 DoFs (3T-1R) actuatedly redundant parallel manipulator based on dual criteria: Dynamics and precision," *IEEE International Conference on Intelligent Robots and Systems*, no. Iros, pp. 1716–1723, 2014.
[53] J. W. F. Cheung and Y. S. Hung, "Modelling and control of a 2-DOF planar parallel manipulator for semiconductor packaging systems," *IEEE/ASME International Conference on Advanced Intelligent Mechatronics, AIM*, vol. 1, pp. 717–722, 2005.
[54] K. Nagai, T. N. Le, Y. Hayashi, and K. Ito, "Proposal of a Redundant Drive Wire Mechanism for producing motions with high acceleration and high precision," *2011 IEEE/SICE International Symposium on System Integration, SII 2011*, pp. 1049–1054, 2011.
[55] S. Kock and W. Schumacher, "A parallel x-y manipulator with actuation redundancy for high-speed and active-stiffness applications," in *Proceedings. 1998 IEEE International Conference on Robotics and Automation (Cat. No.98CH36146)*, vol. 3. IEEE, 1998, pp. 2295–2300.
[56] D. A. Laro, R. Boshuisen, and J. Van Eijk, "Design and control of over-actuated lightweight 450 MM wafer chuck," *Proceedings - ASPE Spring Topical Meeting on Control of Precision Systems, ASPE 2010*, vol. 48, pp. 141–144, 2010.
[57] M. G. E. Schneiders, M. J. G. Van De Molengraft, and M. Steinbuch, "Benefits of over-actuation in motion systems," *Proceedings of the American Control Conference*, vol. 1, no. January, pp. 505–510, 2004.
[58] A. Pil, "Pm demonstreert competenties met ontwikkeling eigen motionplatform." [Online]. Available: https://mechatronicamachinebouw.nl/artikel/pm-demonstreert-competenties-met-ontwikkeling-eigen-motionplatform/
[59] R. M. Schmidt and G. Schitter, *The design of high performance mechatronics high-tech functionality by mulitdisiciplinary systems*. Delft University Press, 2014.
[60] J. H. Park and H. Asada, "Dynamic analysis of noncollocated flexible arms and design of torque transmission mechanisms," *Journal of Dynamic Systems, Measurement and Control, Transactions of the ASME*, vol. 116, no. 2, pp. 201–207, 1994.
[61] K. Mori, T. Munemoto, H. Otsuki, Y. Yamaguchi, and K. Akagi, "A dual-stage magnetic disk drive actuator using a piezoelectric device for a high track density," *IEEE Transactions on Magnetics*, vol. 27, no. 6, pp. 5298–5300, nov 1991.
[62] C.-W. Lee and S.-W. Kim, "An ultraprecision stage for alignment of wafers in advanced microlithography," *Precision Engineering*, vol. 21, no. 2-3, pp. 113–122, sep 1997.
[63] Y. Liu, T. Li, and L. Sun, "Design of a control system for a macro-micro dual-drive high acceleration high precision positioning stage for IC packaging," *Science in China, Series E: Technological Sciences*, vol. 52, no. 7, pp. 1858–1865, 2009.
[64] Y. M. Choi and D. G. Gweon, "A high-precision dual-servo stage using halbach linear active magnetic bearings," *IEEE/ASME Transactions on Mechatronics*, vol. 16, no. 5, pp. 925–931, 2011.
[65] L. Zhang, J. Gao, and X. Chen, "A Rapid Dynamic Positioning Method for Settling Time Reduction Through a Macro-Micro Composite Stage with High Positioning Accuracy," *IEEE Transactions on Industrial Electronics*, vol. 65, no. 6, pp. 4849–4860, 2018.
[66] K. Ramesh Kumar and S. Narayanan, "Active vibration control of beams with optimal placement of piezoelectric sensor/actuator pairs," *Smart Materials and Structures*, vol. 17, no. 5, 2008.
[67] N. Hagood and A. von Flotow, "Damping of structural vibrations with piezoelectric materials and passive electrical networks," *Journal of Sound and Vibration*, vol. 146, no. 2, pp. 243–268, apr 1991.
[68] *CES Edupack*. Granta, 2019.
[69] J.-S. Bae, M. K. Kwak, and D. J. Inman, "Vibration suppression of a cantilever beam using eddy current damper," *Journal of Sound and Vibration*, vol. 284, no. 3-5, pp. 805–824, jun 2005.
[70] L. R. Douat, I. Queinnec, G. Garcia, M. Michelin, and F. Pierrot, "Piezo-actuated vibration attenuation of the parallel robot Par2," *IFAC Proceedings Volumes (IFAC-PapersOnline)*, vol. 7, no. PART 1, pp. 115–120, 2012.
[71] H. Kazerooni, "Direct-drive active compliant end effector (active RCC)," *IEEE Journal on Robotics and Automation*, vol. 4, no. 3, pp. 324–333, jun 1988.
[72] R. Islam, I. Husain, A. Fardoun, and K. McLaughlin, "Permanent-magnet synchronous motor magnet designs with skewing for torque ripple and cogging torque reduction," *IEEE Transactions on Industry Applications*, vol. 45, no. 1, pp. 152–160, 2009.
[73] P. A. McKeown and G. H. Morgan, "Epoxy granite: a structural material for precision machines," *Precision Engineering*, vol. 1, no. 4, pp. 227–229, 1979.

[74] V. Arakelian, “Inertia forces and moments balancing in robot manipulators: a review,” *Advanced Robotics*, vol. 31, no. 14, pp. 717–726, 2017.

[75] R. Raaijmakers, “Besi zoekt snelheidslimiet pakken en plaatsen op,” Sep 2007. [Online]. Available: https://mechatronicamachinebouw.nl/artikel/besi-zoekt-snelheidslimiet-pakken-en-plaatsen-op/

[76] V. Van Der Wijk and J. L. Herder, “Synthesis of dynamically balanced mechanisms by using counter-rotary countermass balanced double pendula,” *Journal of Mechanical Design, Transactions of the ASME*, vol. 131, no. 11, pp. 1 110 031–1 110 038, 2009.

[77] T. Laliberté and C. Gosselin, “Synthesis, optimization and experimental validation of reactionless two-DOF parallel mechanisms using countermechanisms,” *Meccanica*, vol. 51, no. 12, pp. 3211–3225, 2016.

[78] V. Van Der Wijk and J. L. Herder, “Active dynamic balancing unit for controlled shaking force and shaking moment balancing,” *Proceedings of the ASME Design Engineering Technical Conference*, vol. 2, no. PARTS A AND B, pp. 1515–1522, 2010.

[79] J. J. De Jong, B. E. M. Schaars, and D. M. Brouwer, “The influence of flexibility on the force balance quality: a frequency domain approach,” *Proceedings of the 19th international conference of the European Society for Precision Engineering and Nanotechnology*, no. June, pp. 2–5, 2019.

[80] J. J. De Jong, J. P. Meijaard, and V. Van Der Wijk, “The influence of partial force balancing on the shaking moments, contact forces, and precision of a delta robot-like manipulator in a compliant frame,” *Proceedings of the ASME Design Engineering Technical Conference*, vol. 5B-2018, pp. 1–7, 2018.

[81] J. Geng and V. Arakelian, “Design of Partially Balanced Planar 5R Symmetrical Parallel Manipulators via an Optimal Motion Planning,” in *Mechanisms and Machine Science*. Springer International Publishing, 2019, pp. 2211–2220.

[82] P. Lambrechts, M. Boerlage, and M. Steinbuch, “Trajectory planning and feedforward design for electromechanical motion systems,” *Control Engineering Practice*, vol. 13, no. 2, pp. 145–157, feb 2005.

[83] T. Huang, P. Wang, J. Mei, X. Zhao, and D. Chetwynd, “Time Minimum Trajectory Planning of a 2-DOF Translational Parallel Robot for Pick-and-place Operations,” *CIRP Annals*, vol. 56, no. 1, pp. 365–368, 2007.

[84] J. de Jong, J. van Dijk, and J. Herder, “A screw based methodology for instantaneous dynamic balance,” *Mechanism and Machine Theory*, vol. 141, pp. 267–282, nov 2019.

[85] Y. Yazaki, H. Fujimoto, Y. Hori, K. Sakata, A. Hara, and K. Saiki, “Method to shorten settling time using final state control for high-precision stage with decouplable structure of fine and coarse parts,” *IEEJ Transactions on Industry Applications*, vol. 135, no. 3, pp. 227–236, 2015.

[86] H. Butler, “Position Control in Lithographic Equipment: An Enabler for Current-Day Chip Manufacturing,” *IEEE Control Systems*, vol. 31, no. 5, pp. 28–47, 2011.

[87] C. J. Barnard, S. Briot, and S. Caro, “Trajectory Generation for High Speed Pick and Place Robots,” in *Volume 3: Advanced Composite Materials and Processing; Robotics; Information Management and PLM; Design Engineering*. American Society of Mechanical Engineers, jul 2012, pp. 165–174.

[88] H. Li, M. D. Le, Z. M. Gong, and W. Lin, “Motion profile design to reduce residual vibration of high-speed positioning stages,” *IEEE/ASME Transactions on Mechatronics*, vol. 14, no. 2, pp. 264–269, 2009.

[89] N. C. Singer and W. P. Seering, “Preshaping command inputs to reduce system vibration,” *Journal of Dynamic Systems, Measurement and Control, Transactions of the ASME*, vol. 112, no. 1, pp. 76–82, 1990.

[90] T. Singh and W. Sinhose, “Tutorial on input sharping/time delay control of maneuvering flexible structures,” *Proceedings of the American Control Conference*, vol. 3, pp. 1717–1731, 2002.

[91] S. Devasia, E. Eleftheriou, and S. O. Moheimani, “A survey of control issues in nanopositioning,” *IEEE Transactions on Control Systems Technology*, vol. 15, no. 5 SPEC. ISS., pp. 802–823, 2007.

[92] Y. Okazaki, “A Micro Positioning Tool Post using a Piezoelectric Actuator for Diamond Turning Machines,” *Journal of the Japan Society for Precision Engineering*, vol. 54, no. 7, pp. 1375–1380, 1988.

[93] S. Salapaka, A. Sebastian, J. P. Cleveland, and M. V. Salapaka, “High bandwidth nano-positioner: A robust control approach,” *Review of Scientific Instruments*, vol. 73, no. 9, p. 3232, 2002.

[94] P. H. Meckl and W. P. Seering, “Feedforward Control Techniques To Achieve Fast Settling Time in Robots.” *Proceedings of the American Control Conference*, pp. 1913–1918, 1986.

[95] S. Briot, A. Pashkevich, and D. Chablat, “On the optimal design of parallel robots taking into account their deformations and natural frequencies,” *Proceedings of the ASME Design Engineering Technical Conference*, vol. 7, no. PARTS A AND B, pp. 367–376, 2009.

[96] S. Wang, J. Tan, and J. Cui, “Error mechanism analyses of an ultra-precision stage for high speed scan motion over a large stroke,” *Ninth International Symposium on Precision Engineering Measurement and Instrumentation*, vol. 9446, no. March 2015, p. 94462Q, 2015.

[97] S. Mishra, J. Coaplen, and M. Tomizuka, “Precision Positioning of Wafer Scanners Segmented Iterative Learning Control for Nonrepetitive Disturbances,” *IEEE Control Systems*, vol. 27, no. 4, pp. 20–25, 2007.

[98] M. Li, Y. Zhu, K. Yang, L. Yang, and C. Hu, “Data-Based Switching Feedforward Control for Repeating and Varying Tasks: With Application to an Ultraprecision Wafer Stage,” *IEEE Transactions on Industrial Electronics*, vol. 66, no. 11, pp. 8670–8680, 2019.

[99] M. Demetriou, “A numerical algorithm for the optimal placement of actuators and sensors for flexible structures,” in *Proceedings of the 2000 American Control Conference. ACC (IEEE Cat. No.00CH36334)*, no. June. IEEE, 2000, pp. 2290–2294 vol.4.

3

Controllability of dynamically balanced mechanisms: A comparative analysis

Controllability of dynamically balanced mechanisms: A comparative analysis

M.J.J. Zomerdijk, V. van der Wijk

***Abstract*—Settling time of machinery can take up a significant part of the cycle time and depends on the controllability of the mechanism. Not only vibrations in the mechanism affect settling time, but also vibrations in the base. Dynamic balance eliminates vibrations in the base by removing the source of these vibrations. However, balancing, in general, requires the addition of counter-masses and counter-inertias, which can degenerate controllability due to additional mass. The goal of this paper is to compare and evaluate existing balancing principles in order to determine which principle and which configuration has optimal controllability. Selected balancing techniques are: counter-mass (CM), separate counter-rotations (SCR), counter-rotary countermass (CRCM), and the inherently balanced inverted four-bar linkage (IBinv4B). These techniques are applied to a single rotatable link, which is regarded as a building block in mechanism design. Afterwards the principles are evaluated and compared numerically in this reference case. Additionally, the influence of link stiffness on the frequency ratio is investigated by optimization. Results based on the parameter values in the numerical comparison show that SCR-balancing and IBinv4B have 6% higher peak frequency ratios than CRCM-balancing in the reference case. CM-balancing, which is solely force balancing, has significantly higher frequency ratios (more than 50%), showing that force and moment balancing results in lower controllability than force balancing only. Optimizing the link stiffness for CRCM-balancing increased the peak frequency ratio with 14%. On the other hand, frequency ratios of SCR-balancing improved only marginally, therefore CRCM-balancing outperforms SCR-balancing after link stiffness optimization. The peak frequency ratio of the IBinv4B increased with 63% after link stiffness optimization, resulting in comparable frequency ratios as force balancing. Therefore the controllability after optimization is significantly higher than the two other force and moment balancing principles. Additionally, the IBinv4B lacks complex rotary transmissions. A disadvantage of the IBinv4B is the limited range of motion where peak frequency ratios are achieved.**

I. Introduction

High speed machinery requires low cycle times to achieve high production rates. The cycle time is for a significant part determined by the settling time, which is defined as the time to reach and stay within a certain error band of the final position after a motion is initiated. Settling time can be divided into motion time and Ts-Tr time. The former is the time to execute a planned motion, while the latter is the time required for vibrations to die out. Motion time depends on the inertial properties of the mechanism, whereas Ts-Tr time depends on the controllability. Ts-Tr time can, even in highly optimized designs, use up to one third of the settling time [1].

Ts-Tr time depends not only on mechanism itself, but also on the base. The base connects the mechanism to the fixed world and serves as a position reference, vibrations in the frame would therefore affect the precision. Base vibrations are predominantly caused by fluctuating reaction forces and reaction moments excited by the mechanism. In addition, these fluctuating forces and moments can also induce vibrations in other machinery. Dynamic decoupling reduces transmissibility between machines and is commonly achieved by vibrations isolation. Drawback of this technique is reduced absolute precision.

With dynamic balancing, fluctuating forces and moments are removed, therefore removing the source of base vibrations. [2]. Dynamic balance is, in general, achieved by adding counter-masses and counter-inertias. The additional mass and inertia of these elements can degrade natural frequencies. The first natural frequency has a significant impact on the controllability in feedback control, therefore a decrease in natural frequencies results in lower control bandwidth. Time dependent studies of balanced elastic four-bar mechanisms show an increase in vibrations in the mechanism after balancing [3]–[5]. The effect of balancing in the frequency domain is researched for specific cases of a four-bar linkage [6], [7] and a planar force balanced manipulator [8]. In both cases a significant decay in natural frequencies is reported (up to 50%). Despite the reduction in controllability of the mechanism itself, balancing can improve settling time. There are indications that balancing can reduce the settling time by 94% [9], [10].

The goal of this paper is to compare existing balancing principles in order to determine which principle and which configuration has optimal controllability. With the aim to make a fair comparison, these principles are applied to a single rotatable link, which is regarded as a representative building block in machine design.

The focus is on fully passive balanced solutions. Active balanced solutions are more flexible, but they require additional control and drives which increase cost and complexity [11]. In addition, active moment balancing only results in a reduction of around 90% in reaction moments [1]. Partial balanced solutions require a task specific approach for each application, therefore it is difficult to conduct an universal comparison [8]. In addition, the performance of partial balanced solutions depend on the base properties, which requires a significant amount of assumptions.

This paper is structured as follows. In section II the fundamentals and reference mechanism of this study are introduced. Section III introduces the selected balancing principles and their balancing conditions. Section IV applies these principles in a numerical example and investigates the impact on the controllability. Discussion and conclusion is

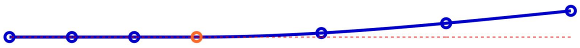

(a) Mode shape of the first natural frequency assuming perfect tracking. The actuated joint, which is indicated in orange, is fixed in this case. The elements on the left side of the actuated joint are not influenced by the excited mode shape on the right side, which means they are decoupled from each other.

(b) Mode shape of the first rotary unconstrained natural frequency after the rigid body mode. The actuated joint, which is indicated in orange, is released in this case. The elements on the left are now coupled with elements on the right.

Fig. 1: Comparison between mode shapes when assuming perfect tracking and when the actuated joint is released. Mode shapes are modelled in Spacar.

formulated in sections V and VI, respectively.

II. Methods

The influence of balancing on inertial properties and controllability is assessed by three parameters: 1) the reduced moment of inertia, 2) the moving mass of the mechanism, and 3) the first rotational unconstrained natural frequency. The reduced moment of inertia is a measure for the kinetic energy stored in the mechanism during motion. Actuator requirements can therefore be derived from the reduced moment of inertia [12]. Natural frequencies depend on the mass, inertia, and stiffness of the mechanism, modal analysis is used to calculate these frequencies. Modal analysis assumes perfect control over the actuated joint angle (perfect tracking) and therefore an infinitely stiff actuator is required [8]. In reality the virtual stiffness of an actuator is determined by the feedback loop performance, which is often limited by the first natural frequency. Additionally, perfect tracking decouples elements which are attached to the actuated joint from each other (Fig. 1a). This means that there is no transmissibility between elements directly attached to the actuated joint. To resolve these issues and omit feedback loop performance, chosen is to analyse the rotational unconstrained natural frequencies. This means the actuated joint is released (Fig. 1b).

A. Conditions for dynamic balancing of mechanisms

Dynamic balancing can be divided into shaking force and shaking moment balancing. A shaking force balanced mechanism has a stationary centre of mass (CoM) with respect to the base, which eliminates fluctuating reaction forces exerted on the base. A stationary CoM means the sum of all linear momenta equals zero, as shown in Equation 1.

$$p = \sum_i m_i \dot{r_i} = m_{tot}\dot{r}_{CoM} = 0 \tag{1}$$

With i denoting the element number, $\dot{r_i}$ the position of the CoM of the element, and m_i the mass of the element.

A shaking moment balanced mechanism eliminates fluctuating reaction moments on the base. In accordance with Euler's second law of motion, this requires a constant angular momentum, which is described by Equation 2.

$$\dot{H}_0 = \sum_i r_i \times (m_i \ddot{r_i}) + I_i \ddot{\theta}_i = M_0 = 0 \tag{2}$$

With M_0 denoting the reaction moment and I_i the mass moment of inertia (will be referred to as inertia) of the element. The angular acceleration of the element is denoted with $\ddot{\theta}_i$.

Satisfying both Equation 1 and 2, results in a dynamically balanced mechanism. A shaking force balanced mechanism is achieved by satisfying only Equation 1.

B. Reference mechanism

Aimed to make a fair comparison between multiple balancing principles, it is chosen to apply them to a rotatable link (pendulum). The rotatable link is be regarded as a representative building block in mechanism design. For instance, Delta robots [13] are based on three parallel dyads (double pendulums) and multiple linkages are based on rotatable links [14]. It is expected that conclusions for a single rotatable link are also applicable in the design of balanced mechanisms with multiple links and multiple degree of freedom. Fig. 2 shows a rotatable link with length L, distributed link mass μ, tip mass m and tip inertia I.

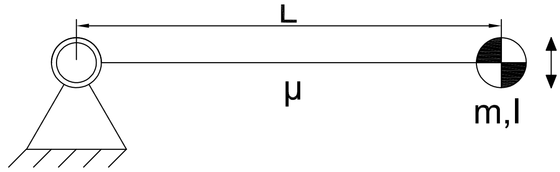

Fig. 2: Single pendulum as reference mechanism.

Inertial properties and natural frequencies of the reference mechanism in Fig. 2 can be calculated with Equation 3.

$$\begin{aligned}
\text{Reduced inertia:} \quad & I_\theta^{0red} = mL^2 + I + \frac{1}{3}\mu L^3 \\
\text{Total mass:} \quad & m_{tot}^0 = m + \mu L \\
\text{Natural frequencies:} \quad & f_{im}^0 = \frac{\lambda_{im}^2}{2\pi L^2}\left(\frac{EJ_{zz}}{\mu L}\right)^{1/2}
\end{aligned} \tag{3}$$

With im denoting the mode number, E the elastic modulus of the material and J_{zz} the second moment of inertia of the link. λ_i is calculated by solving Equation 4 [15].

$$\begin{aligned}
&(1 - \frac{m}{\mu L}\frac{I}{\mu L^3})(\tan(\lambda_{im}) - \tanh(\lambda_{im})) \\
&+2\lambda_{im}[\frac{m}{\mu L}\tan(\lambda_{im})\tanh(\lambda_{im}) + \frac{I}{\mu L^3}\lambda_{im}^2] = 0
\end{aligned} \tag{4}$$

III. Comparison of mechanisms

Common balancing principles were collected in a comparative analysis of mass and inertia by Van der Wijk [16]. These balancing principles are: counter-mass (CM), separate counter-rotations (SCR), and counter-rotating counter-mass (CRCM). SCR-balancing and CRCM-balancing result in a dynamically balanced mechanism, while CM balancing only results in a force balanced mechanism. Less common is the balancing of a link with an inherently balanced inverted four-bar linkage (IB-inv4B) [17]. Distinctive feature of this mechanism compared to SCR-balancing and CRCM-balancing is that this mechanism is inherently balanced. Therefore the IBinv4B does not rely on rotary transmissions, which can reduce backlash, compliance, inertia and costs.

All compared mechanisms are planar and modelled with fully elastic links, joints are assumed rigid and massless. Modal analysis is conducted with the help of Spacar [18], a numerical flexible multi-body software package based on the Euler Bernoulli beam theory. Modal analysis is conducted in 2D, therefore out-of-plane vibrations are not taken into account. However, the natural frequencies associated with out-of-plane vibrations are equal or higher than their in-plane equivalents due to the rigid joints and cylindrical shaped links.

Balancing conditions for CM, SCR, and CRCM are known for a rotatable link with lumped mass [16]. These conditions are extended to incorporate link mass and inertia. An asterisk (.)* denotes additional balancing elements. Additional links and extension of links have equal properties to the link in the reference mechanism. To reduce complexity, non-uniform distributed masses in the simulations are modelled as solid discs with density ρ, thickness t and radius R. The inertia and mass of the disk can be calculated with Equation 5.

$$\begin{aligned} m &= \rho \pi t R_i^2 \\ I &= \frac{1}{2} m_i R_i^2 \end{aligned} \tag{5}$$

A. Counter-mass balancing

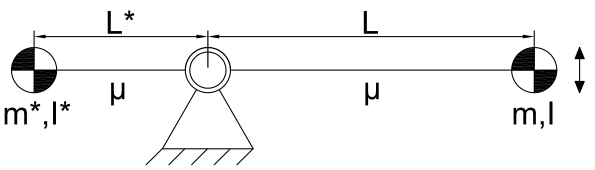

Fig. 3: Counter-mass balanced pendulum.

Adding a counter-mass to the reference mechanism in Fig. 2, results in a force balanced mechanism (Fig. 3). The counter-mass is denoted with mass m^*, inertia I^*, and position L^*. Although force balancing does not result in a dynamically balanced mechanism, it is used as an additional reference. Force balancing condition is listed in Equation 6, inertial properties are listed in Equation 7

$$\text{Force balance:} \quad mL + \frac{1}{2}\mu L^2 - \frac{1}{2}\mu L^{*2} - m^* L^* = 0 \tag{6}$$

$$\begin{aligned} \text{Reduced inertia:} \quad I_\theta^{red} &= mL^2 + I + \frac{1}{3}\mu L^3 + \frac{1}{3}\mu L^{*3} \\ &\quad + I^* + m^* L^{*2} \\ \text{Total mass:} \quad m_{tot} &= m + \mu L + \mu L^* + m^* \end{aligned} \tag{7}$$

B. Separate counter-rotation balancing

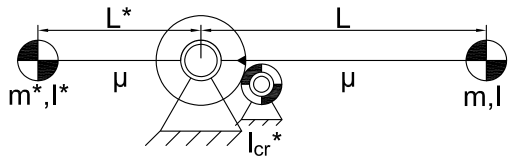

Fig. 4: Separate counter-rotations balanced pendulum.

Dynamic balance with the SCR principle is achieved by adding a counter-inertia at the base of a force balanced mechanism. The counter-inertia is denoted with I_{cr}^* (Fig. 4) and connected to the link with a transmission. The transmission inverts the rotation, which makes the counter-inertia counter-rotate with respect to the link. Equation 8 defines the balancing conditions for SCR-balancing, inertial properties can be calculated with Equation 9.

$$\begin{aligned} \text{Force balance:} \quad & mL + \frac{1}{2}\mu L^2 - \frac{1}{2}\mu L^{*2} - m^* L^* = 0 \\ \text{Moment balance:} \quad & mL^2 + I + \frac{1}{3}\mu L^3 + \frac{1}{3}\mu L^{*3} + I^* \\ & + m^* L^{*2} + I_{cr}^* k_{scr} = 0 \end{aligned} \tag{8}$$

$$\begin{aligned} \text{Reduced inertia:} \quad I_\theta^{red} &= mL^2 + I + \frac{1}{3}\mu L^3 + \frac{1}{3}\mu L^{*3} \\ &\quad + I^* + m^* L^{*2} + I_{cr}^* k_{scr}^2 \\ \text{Total mass:} \quad m_{tot} &= m + \mu L + \mu L^* + m^* + m_{cr}^* \end{aligned} \tag{9}$$

In Equation 8, the factor k_{scr} is equal to the transmission ratio, which can be calculated with $k_{scr} = \frac{d_0}{d_{scr}}$. Where d_0 is the diameter of the gear attached to the link and d_{scr} the diameter of the gear which is attached to the counter-inertia.

Duplicate mechanisms are regarded as a special case of SCR-balancing. A duplicate mechanism is achieved by replacing the counter-inertia for an identical force balanced link. Duplicate mechanisms have better inertial properties, but require more space [16].

C. Counter-rotary counter-mass balancing

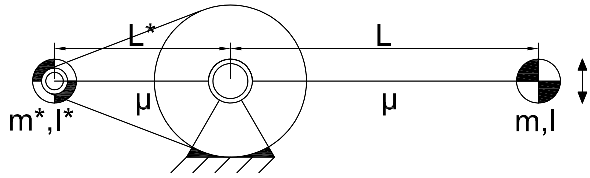

Fig. 5: Counter-rotating counter-mass balanced pendulum.

In CRCM-balancing, the inertia of the counter-mass is used as a counter-inertia (Fig. 3). This reduces mass and inertia, because the counter-mass and counter-inertia are combined in a single element. The balancing conditions are listed in Equation 10, inertial properties can be calculated with Equation 11.

$$\begin{aligned} &\text{Force balance:} \quad mL + \frac{1}{2}\mu L^2 - \frac{1}{2}\mu L^{*2} - m^* L^* = 0 \\ &\text{Moment balance:} \quad mL^2 + I + \frac{1}{3}\mu L^3 + \frac{1}{3}\mu L^{*3} + I^* \\ &\qquad +m^* L^{*2} + I^* k_{crcm} = 0 \end{aligned} \tag{10}$$

$$\begin{aligned} &\text{Inertia:} \quad I_\theta^{red} = mL^2 + I + \frac{1}{3}\mu L^3 \\ &\quad +\frac{1}{3}\mu L^{*3} + I^* k_{crcm}^2 + m^* L^{*2} \\ &\text{Total mass:} \quad m_{tot} = m + \mu L + \mu L^* + m^* \end{aligned} \tag{11}$$

In Equation 10, the transmission ratio k_{crcm} can be obtained with $k_{crcm} = 1 - \frac{d_0}{d_{crcm}}$. Where d_0 is the diameter of gear connected to the base and d_{crcm} the gear diameter connected to the CRCM [19].

D. IBinv4B

In contrast to the other dynamic balancing principles in this study, does the IBinv4B not rely on separate counter-rotating elements or rotary transmissions. In Fig. 6 the original link is extended with length L_1, at the end is the second (coupler) link attached with length L_2. The third link is connected to a base attached revolute joint and the coupler link, L_3 denotes the distance between the base pivot and the coupler link. Two balancing masses with mass m_i^*, inertia I_i^*, and position r_i^* are added along the second and third link.

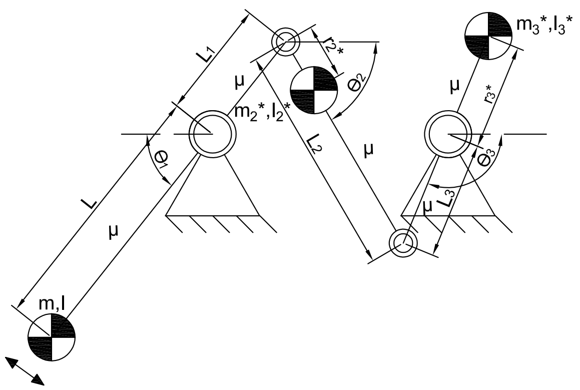

Fig. 6: Inherently balanced inverted four-bar linkage (IBinv4B).

Berkof and Lowen derived the conditions to achieve shaking force balance in a four-bar linkage [20]. These conditions are listed in Equation 12. In addition to this equation, all the links need to have a CoM which is located on the centre line of the link (as shown in Fig. 6).

$$\begin{aligned} &\text{Force balance:} \\ &r_2 = L_2\left(1 - \frac{m_1 r_1}{m_2 L_1}\right), \quad r_3 = \frac{m_2 r_2 L_3}{m_3 L_2} \end{aligned} \tag{12}$$

In Equation 12, r_i denotes the CoM of the link and m_i the total mass of the link including counter-masses and tip mass. Ricard and Gosselin discovered three solutions to dynamically balance four-bar linkages [17], of these solutions the linkage shown in Fig. 6 is selected. This linkage is chosen because the mass distribution has better potential for high natural frequencies. The IBinv4B mechanism is achieved by satisfying both Equation 12 and 13.

$$\begin{aligned} &\text{Moment balance:} \\ &L_1 = L_3, \quad d = L_2, \\ &I_2 = m_2(L_2 r_2 - r_2^2) - I_{c1}, \\ &I_3 = -m_3(L_3 r_3 + r_3^2) + I_{c1}, \\ &I_{c1} = I_1 + m_1(r_1^2 + r_1 L_1) \end{aligned} \tag{13}$$

In Equation 13 I_i denotes the moment of inertia of the i_{th} link including counter-masses and tip load. d denotes the distance between the revolute joints attached to the base. Wu and Gosselin proved that satisfying Equation 12 and 13 also results in a mechanism which has constant inertia for in-plane rotations [21]. Further research had the aim to optimize the mass [22] and actuation torque [23]. Briot extended the mechanism with the help of Assur groups to generate a method for balancing general four-bar linkages [24].

Inertial properties of Fig. 6 are derived with the help of the kinetic energy of the mechanism (derived in the Appendix (section VII-C)). Equations for the kinetic energy of a four-bar linkage are derived by Berkhof [25]. Inertial properties of the balanced mechanism are listed in Equation 14.

$$\begin{aligned} &\text{Reduced inertia:} \quad I_\theta^{red} = I_1^{red} + I_2^{red} k_2^2 + I_3^{red} k_3^3 + m_2 L_1^2 \\ &\qquad +2 m_2 l_1 \cos(\theta_2 - \theta_1) k_2, \\ &k_3 = \frac{-L_2 \sin(\theta_1 - \theta_3)}{L_3 \sin(\theta_2 - \theta_3)}, \quad k_2 = \frac{-L_2 \sin(\theta_1 - \theta_2)}{L_3 \sin(\theta_2 - \theta_3)} \\ &\text{Total mass:} \quad m_{tot} = m + \mu L + \mu L_1 + m_2^* + \mu L_2 \\ &\qquad +\mu L_3 + \mu r_{cm3} + m_3^* \end{aligned} \tag{14}$$

In Equation 14, θ_i denotes the angle between the horizontal axis and the i_{th}. k_2 and k_3 are the transmission ratios of the second and third link with respect to the first link.

IV. Numerical comparison

Links are modelled as tubes with outer radius r_b and wall thickness t_b. Parameter values which are used in the numerical comparison are listed in Table 1. When optimization is applied, it is focussed on the optimal outer radius of the tube with constant wall thickness.

Table 1: Parameter values in the numerical comparison

$L = 1$ (m)	$r_b = 25$ (mm)	$t_b = 5$ (mm)
$m = 1$ (kg)	$\mu = 1.9$ (kg/m)	$t_{cm} = 100$ (mm)
$\rho = 2700$ (kg/m^3)	$E = 67.5$ (Gpa)	$G = 25.2$ (Gpa)

Solving Equation 3, with the parameters of Table 1, results in a first unconstrained natural frequency of 143.06 Hz. In Spacar, each beam is modelled with three beam elements, resulting in a first natural frequency of 142.94 Hz. Compared to the analytical and numerically converged solution is the error in both cases less than 0.1% (see Appendix (section VII-A)). Comparison is conducted by using the dimensionless ratios in Equation 15.

$$\begin{aligned} \text{Mass ratio:} \quad & \hat{m} = \frac{m_{tot}}{m_{tot}^0} \\ \text{Inertia ratio:} \quad & \hat{I} = \frac{I_\theta^{red}}{I_\theta^{0red}} \\ \text{Frequency ratio:} \quad & \hat{f} = \frac{f}{f^0} \end{aligned} \tag{15}$$

Variables denoted with a superscript 0 correspond with the reference mechanism, with $m_{tot}^0 = 2.9$ kg, $I_\theta^{0red} = 1.13$ kg/mm^2, and $f^0 = 142.94$ Hz. Rotary transmissions (for example belts or gears) are modelled rigid and massless to reduce the number of parameters. In transmissions one of the gears or pulleys is fixed to a diameter of 10 mm, while the other is dependent on the transmission ratio. Due to the large dependency on both inertia and mass, frequency ratio's are only applicable for comparison in the reference case. A different reference case results in different frequency ratios.

A. Counter-mass balancing

The position of the counter-mass (L^*) is made variable, resulting frequency, mass and inertia ratios are shown in Fig. 7.

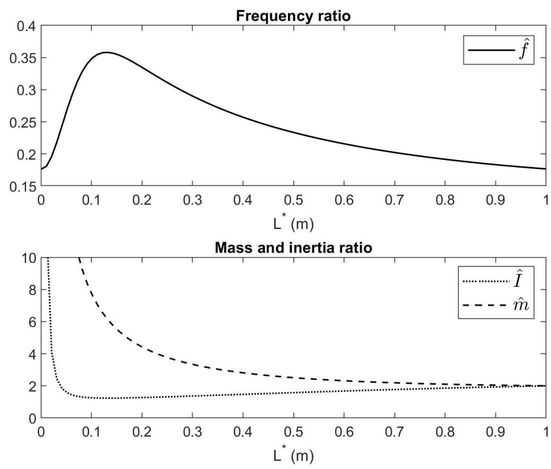

Fig. 7: Influence of length L^* on frequency, inertia, and mass ratios in counter-mass balancing.

As can been seen in Fig. 7, a dependency between the frequency and inertia ratio can be noticed. The frequency ratio is optimal when the inertia ratio is minimized. When L^* equals L the rotational joint remains stationary, which means the natural frequency is equal to the constrained first natural frequency of the reference mechanism. The same behaviour is visible at high inertia ratios, which virtually fixes the rotary joint.

B. SCR-balancing

Compared to force balancing, the reduced inertia in SCR-balancing doubles at equal lengths of L^* with a transmission ratio of 1. As noticed with force balancing, minimizing the reduced inertia results in optimal natural frequencies, imposing that a low transmission ratio is beneficial. SCR-balancing will, in general, never outperform force balancing due to the additional inertia required for shaking moment balance. Simulation results are shown in Fig. 8.

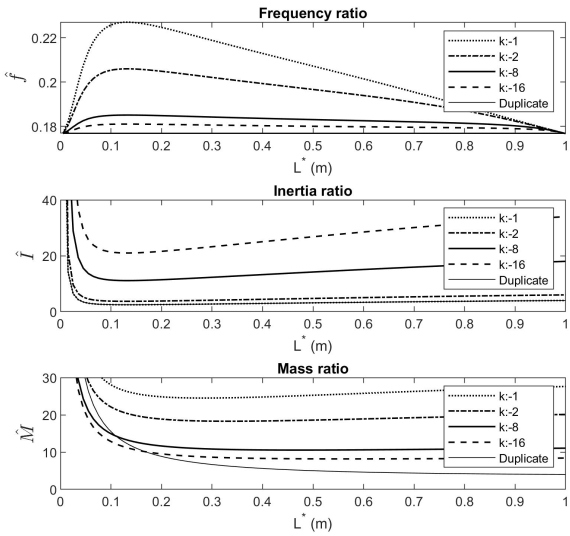

Fig. 8: Influence of length L^* on frequency, inertia, and mass ratios in separate counter-rotation balancing with multiple transmission ratios.

Fig. 8 shows an optimal frequency ratio is achieved at equal length of L^* as force balancing. This position has minimal reduced inertia and a frequency ratio of 0.226. Duplicate mechanisms have a constant frequency ratio due to mirrored mode shapes, resulting in a stationary rotary joint. The mirrored mode shapes also result in a harmonically balanced mechanism, because reaction forces and moments exerted by the vibrations cancel each other out. Increasing the stiffness of the link at L^* has no significant influence on the frequency ratio in SCR-balancing, meaning the inertia of the counter-inertia is limiting the frequency ratio. Reducing the mass by increasing the transmission ratio impacts natural frequencies negatively, due to higher reduced inertia. This makes SCR-balancing less suitable for low mass applications.

C. CRCM-balancing

The reduced inertia of CRCM-balancing is lower than SCR-balancing, which should indicate higher natural frequencies. On the other hand, the counter-inertia is attached to an elastic link and transmission dimensions limit the minimum length of L^*. The shape of the CRCM is defined by the required mass and inertia to satisfy the balancing equations, which can result in inconvenient form factors. Some resulting form factors may even not be manufacturable and require to alter the length of L^* or the transmission ratio. Manufacturability of the counter-mass in CRCM-balancing is not included in this study, but awareness of this problem in early design can prevent poor controllability. Mass ratios in CRCM-balancing are equal to force balancing in Fig. 7. Resulting frequency inertia ratios are shown in Fig. 9.

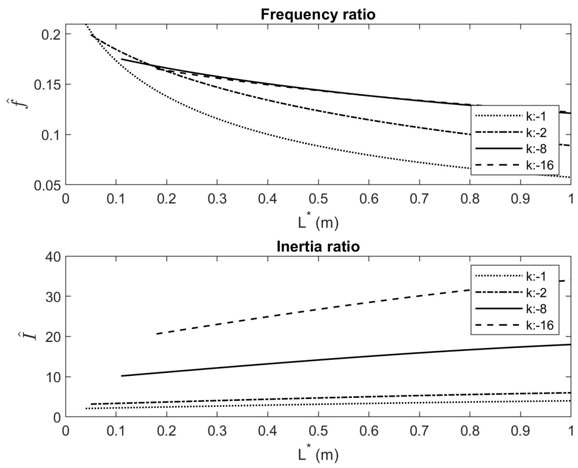

Fig. 9: Influence of length L^* on frequency and inertia ratios in counter-rotating counter-mass balancing with multiple transmission ratios.

Fig. 9 shows the maximum frequency ratio (0.210) is lower than SCR, indicating that the compliance of the balancing link limits controllability. Increasing the outer diameter of this link with a factor 10 increases the frequency ratio by around 14% (to 0.239). In this case CRCM-balancing outperforms SCR-balancing. The frequency ratio can also be improved by increasing the size of the gears in the transmission, which reduces reaction forces exerted on the link. Disadvantage of this solution is that the inertia will also increase with larger gear. Higher transmission ratios are not advisable, because they add inertia and reduce the frequency ratio, while the mass is not influenced. Non-optimal frequency ratio's are much lower than SCR and show the importance to optimize the balancing link stiffness.

D. IBinv4B

In contrast to the previous open loop mechanisms, four-bar mechanisms are closed loop. Additionally, the IBinv4B does not rely on rotary transmissions which, although assumed ideal in this research, add compliance, backlash, and mass. The results of the IBinv4B depend on the lengths L_1, L_2, and angle θ. First, the influence of L_1 and L_2 is studied by altering angle θ to a position where the frequency ratio is maximal. Frequency ratios for the IBinv4B are shown in Fig. 10 and inertia ratios in Fig. 11.

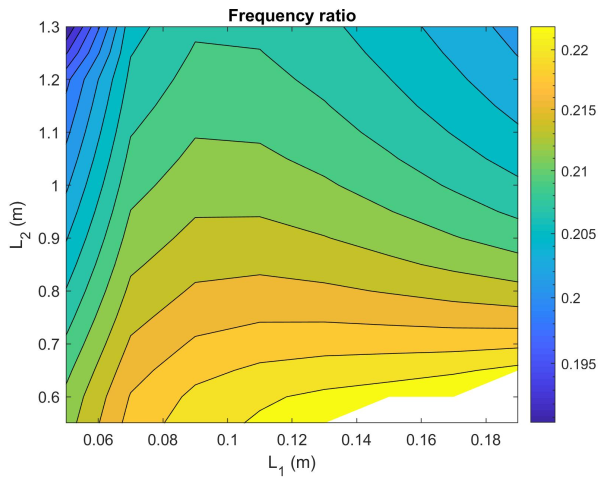

Fig. 10: Frequency ratios of the IBinv4B when L_1 and L_2 are variable.

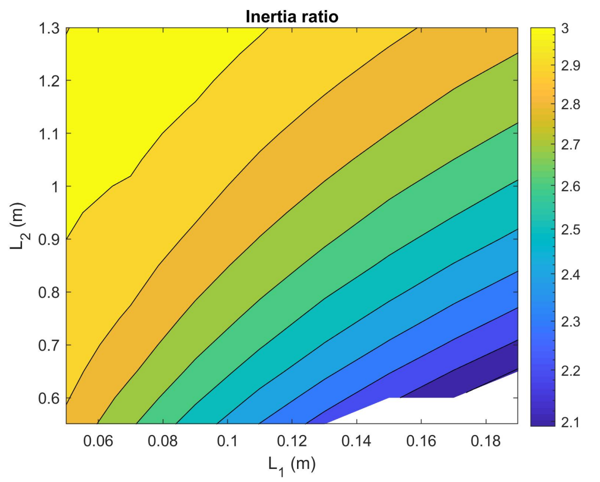

Fig. 11: Inertia ratios of the IBinv4B when L_1 and L_2 are variable.

The frequency ratio plot in Fig. 10 shows that L_2 has a higher influence on the frequency ratio than L_1. The peak frequency ratio (0.224) is comparable to SCR-balancing, while the inertia ratio is comparable to CRCM-balancing with a transmission ratio of 1. In contrast to the other balancing principles, does the frequency and inertia ratio depend on angle θ_1. For further analysis the length of L_1 is fixed to 0.15 m and the angle θ_1 is made variable.

Fig. 12 shows that the frequency ratio decays significantly when the mechanism nears singular positions (at 0 and 180

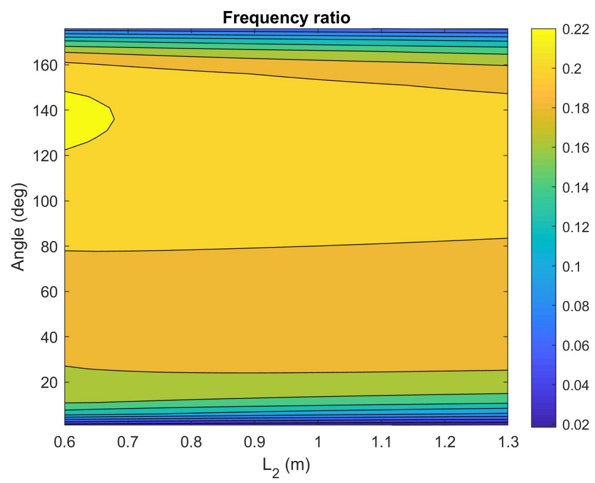

Fig. 12: Frequency ratios of the IBinv4B when L_2 and θ_1 are variable.

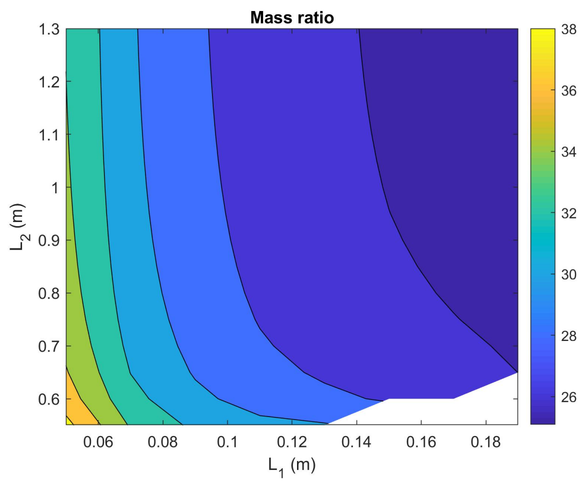

Fig. 14: Mass ratio of IBinv4B at different lengths of L_1 and L_2

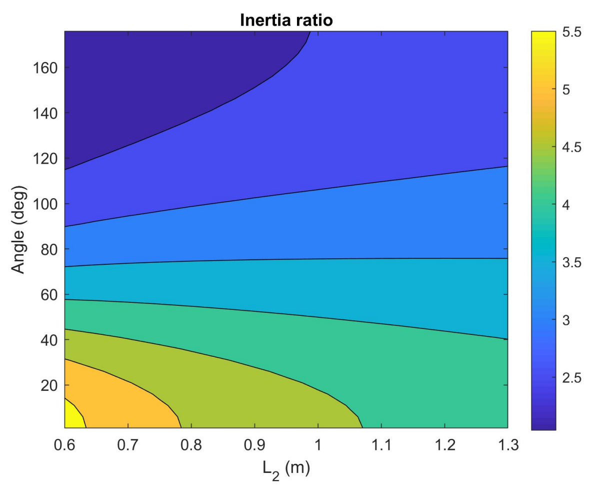

Fig. 13: Inertia ratios of the IBinv4B when L_2 and θ_1 are variable.

degrees). A range of motion of 90 degrees is feasible when a decay of maximal 10% in frequency ratio is accepted. The inertia ratio differs with the angle θ_1. Lower inertia ratios are achieved around the same position of the highest frequency ratio (Fig. 13). The decay in frequency ratios at smaller angles of θ_1 is caused by a predominantly transverse load on link 1 when the mode shape is excited. At larger angles of θ_1 the load becomes predominately longitudinal, in this direction the link has significantly higher stiffness.

Fig. 14 shows an inverse dependency between the mass of the mechanism and the length of L_1. Mass ratios are comparable to SCR-balancing, therefore CRCM-balancing is more suitable in low mass applications. Although reducing the thickness of the counter-mass in the third link can significantly reduce the mass ratio. This is mainly caused by the high inertia required in the third link to satisfy the balancing conditions.

By optimizing link stiffness of the IBinv4B mechanism, the frequency ratio can be increased. An improvement of 63% in peak frequency ratio is achievable for the mechanism in this paper, resulting in a frequency ratio comparable to force balancing (0.366). In this case L_1 and L_2 are 0.316 m and 0.802 m, respectively. The outer diameter at the extension of the first link is doubled, the outer diameter of the second link is increased with 30%, and the third link has a 3.4 times larger outer diameter. This shows most important sections which determine frequency ratios are along the length L_1 and third link. The potential to improve frequency ratios is therefore significantly higher than SCR-balancing or CRCM-balancing. In addition, after optimization the IBinv4B has a more than 50% higher frequency ratio compared to CRCM-balancing after optimization.

V. Discussion

A single rotatable link was in this study assumed as a building in mechanism design. Stacking multiple links in series results in a multiple DoF mechanism. The tip mass and inertia in a proximate link are in this case the mass and inertia of a distal link. A dynamically balanced link has constant mass, CoM, and inertia during in-plane rotations of the whole mechanism [19], [21]. As a result a dynamically balanced link behaves, when modelled rigidly, as a point mass. Elasticity in a balanced link can result in unbalance due to not satisfying the mass distribution required for dynamical balance. This effect can occur in high acceleration applications, but in this case balancing distal links significantly degenerates controllability [8]. Resorting to a parallel architecture which is based on a pantograph or parallelogram is therefore recommended [1], [26]. With this architecture only the proximate links need to be balanced to achieve a dynamically balanced mechanism. As these proximate links are single rotatable links the results of this study stay applicable.

Modelling non-uniform distributed masses as solid discs results in non-optimal performance. In practice more complex shapes are preferable to increase or reduce inertia and mass. Two cases can be distinguished: 1) maximizing mass while minimizing inertia and 2) maximizing inertia while minimizing mass. In the former case increasing the out-of-plane thickness will improve performance, while in the latter case a cylindrical shell or tube will be better suited.

The controllability is rated with the help of unconstrained natural frequencies, which are sensitive to the inertia of the load. Higher frequency ratios are obtainable when a high inertia load is attached. This is mainly caused by a lower natural frequency in the reference mechanism. Therefore the results are only valid for comparison between balancing principles. In addition, the constrained mode shapes give more information during design, as they are more convenient to interpret. The significance of a mode shape in a certain direction can be quantified with mode participation factors. Mode participation factors are a measure of the stored energy in a mode. Combining constrained natural frequencies with mode participation factors can therefore result in a more intuitive method to quantify controllability in balanced mechanisms.

All rotary transmissions in this research are modelled as rigid and massless. This choice is made because backlash, compliance, and additional mass can influence natural frequencies significantly and make results less clear. Results of SCR-balancing and CRCM-balancing are therefore a theoretical maximum, while the IBinv4B is closer to reality.

Optimization of stiffness in this study is only focussed on the outer radius of the tubes. Optimizing the shape and all dimensions will result in higher natural frequencies. When the transverse stiffness is not uniform any more, out-of-plane vibrations should also be analysed.

Elasticity in the base is omitted in this study. In SCR-balancing and the IBinv4B, the two base attached revolute joints are connected rigidly. In reality the base will have limited stiffness, which can result in reduced natural frequencies.

VI. Conclusion

In this paper CM balancing, SCR-balancing, CRCM-balancing and the IBinv4B are numerically compared in terms of controllability and inertial properties. The comparison involved the frequency, inertia, and mass ratios, which asses the performance relative to a reference mechanism. The locations of balancing masses were made variable to analyse the effect on frequency and inertia ratios. Additionally, the influence of link stiffness on the frequency ratio is investigated by optimization.

The frequency ratio of all compared balancing principles show a strong dependency on the inertia ratio, therefore a decay in controllability can be detected when reduced inertia increases. Results based on the parameter values in the numerical comparison show that SCR-balancing and IBinv4B have 6% higher peak frequency ratios than CRCM-balancing in the reference case. CM-balancing, which is solely force balancing, has significantly higher frequency ratios (more than 50%), showing that force and moment balancing results in lower controllability than force balancing only.

Optimizing the balancing link stiffness for CRCM-balancing increased the peak frequency ratio with 14%. In contrast, frequency ratios of SCR-balancing improved only marginally, therefore CRCM-balancing outperforms SCR-balancing after link stiffness optimization. The peak frequency ratio of the IBinv4B increased with 63% after link stiffness optimization, resulting in comparable frequency ratios as force balancing (without optimization). This is mainly because the IBinv4B is closed loop and masses are located at simply supported links or close to the base. Additionally does the IBinv4B not rely on rotary transmissions, which removes additional mass, compliance, and backlash. A disadvantage of the IBinv4B is the limited range of motion where the peak frequency ratios are reached. In case full rotations are required, resorting to SCR-balancing or CRCM-balancing is recommended.

In order to decrease settling time and improve cycle time the IBinv4B shows significant higher potential than SCR- and CRCM-balancing. Key into achieving significantly higher natural frequencies is to optimize stiffness in the first and third link.

References

[1] J. Karidis, G. McVicker, J. Pawletko, L. Zai, M. Goldowsky, R. Brown, and R. Comulada, "The Hummingbird minipositioner-providing three-axis motion at 50 g's with low reactions," in *Proceedings 1992 IEEE International Conference on Robotics and Automation*, vol. 1. IEEE Comput. Soc. Press, 1992, pp. 685–692.

[2] V. van der Wijk, "Methodology for analysis and synthesis of inherently force and moment-balanced mechanisms: theory and applications," Ph.D. dissertation, University of Twente, Enschede, The Netherlands, apr 2014.

[3] F. Xi and R. Sinatra, "Effect of dynamic balancing on four-bar linkage vibrations," *Mechanism and Machine Theory*, vol. 32, no. 6, pp. 715–728, aug 1997.

[4] M. J. Walker and R. S. Haines, "An experimental study of the effects of counterweights on a six-bar chain," *Mechanism and Machine Theory*, vol. 17, no. 6, pp. 355–360, 1982.

[5] J. P. Meijaard and V. van der Wijk, "On the Dynamic Balance of a Planar Four-Bar Mechanism with a Flexible Coupler," in *Mechanisms and Machine Science*, 2019, vol. 73, pp. 3037–3046.

[6] A. Martini, M. Troncossi, and A. Rivola, "Elastodynamic effects of mass-balancing: Experimental investigation of a four-bar linkage," *Advances in Mechanical Engineering*, vol. 2013, 2013.

[7] A. Martini, M. Troncossi, M. Carricato, and A. Rivola, "Elastodynamic behavior of balanced closed-loop mechanisms: Numerical analysis of a four-bar linkage," *Meccanica*, vol. 49, no. 3, pp. 601–614, 2014.

[8] J. J. De Jong, B. E. M. Schaars, and D. M. Brouwer, "The influence of flexibility on the force balance quality: a frequency domain approach," *Proceedings of the 19th international conference of the European Society for Precision Engineering and Nanotechnology*, no. June, pp. 2–5, 2019.

[9] H. F. Menschaar, A. B. Ariens, J. L. Herder, and B. M. Bakker, "Five-bar mechanism with dynamic balancing means and method for dynamically balancing a five-bar mechanism," WIPO Patent WO2 006 080 846A1, 2006.

[10] R. Raaijmakers, "Besi zoekt snelheidslimiet pakken en plaatsen op," Sep 2007. [Online]. Available: https://mechatronicamachinebouw.nl/artikel/besi-zoekt-snelheidslimiet-pakken-en-plaatsen-op/

[11] V. Van Der Wijk and J. L. Herder, "Active dynamic balancing unit for controlled shaking force and shaking moment balancing," *Proceedings of the ASME Design Engineering Technical Conference*, vol. 2, no. PARTS A AND B, pp. 1515–1522, 2010.

[12] H. Dresig and F. Holzweißig, *Dynamics of Machinery*. Berlin, Heidelberg: Springer Berlin Heidelberg, 2010.

[13] R. Clavel, “Device for the movement and positioning of an element in space,” US Patent US4 976 582A, 1990.

[14] K.-H. Grote and J. Feldhusen, *Dubbel: Taschenbuch für den Maschinenbau*. Springer Berlin, 2011.

[15] T. W. Lee, “Vibration Frequencies for a Uniform Beam With One End Spring-Hinged and Carrying a Mass at the Other Free End,” *Journal of Applied Mechanics*, vol. 40, no. 3, pp. 813–815, sep 1973.

[16] V. Van der Wijk, B. Demeulenaere, C. Gosselin, and J. L. Herder, “Comparative Analysis for Low-Mass and Low-Inertia Dynamic Balancing of Mechanisms,” *Journal of Mechanisms and Robotics*, vol. 4, no. 3, pp. 1–8, 2012.

[17] R. Ricard and C. M. Gosselin, “On the Development of Reactionless Parallel Manipulators,” *ASME Design Engineering Technical Conferences and Computers and Information in Engineering Conference*, no. September, pp. 1–10, 2000.

[18] J. B. Jonker and J. P. Meijaard, “SPACAR — Computer Program for Dynamic Analysis of Flexible Spatial Mechanisms and Manipulators,” in *Multibody Systems Handbook*. Berlin, Heidelberg: Springer Berlin Heidelberg, 1990, pp. 123–143.

[19] V. van der Wijk, J. L. Herder, and B. Demeulenaere, “Comparison of various dynamic balancing principles regarding additional mass and additional inertia,” *Journal of Mechanisms and Robotics*, vol. 1, no. 4, pp. 1–9, 2009.

[20] R. S. Berkof and G. G. Lowen, “A New Method for Completely Force Balancing Simple Linkages,” *Journal of Engineering for Industry*, vol. 91, no. 1, pp. 21–26, feb 1969.

[21] Y. Wu and C. M. Gosselin, “Synthesis of reactionless spatial 3-DoF and 6-DoF mechanisms without separate counter-rotations,” *International Journal of Robotics Research*, vol. 23, no. 6, pp. 625–642, 2004.

[22] C. M. Gosselin, F. Vollmer, G. Côté, and Y. Wu, “Synthesis and design of reactionless three-degree-of-freedom parallel mechanisms,” *IEEE Transactions on Robotics and Automation*, vol. 20, no. 2, pp. 191–199, 2004.

[23] Q. Jiang and C. M. Gosselin, “Dynamic Optimization of Reactionless Four-Bar Linkages,” *Journal of Dynamic Systems, Measurement, and Control*, vol. 132, no. 4, pp. 1–11, jul 2010.

[24] S. Briot and V. Arakelian, “Complete shaking force and shaking moment balancing of in-line four-bar linkages by adding a class-two RRR or RRP Assur group,” *Mechanism and Machine Theory*, vol. 57, pp. 13–26, 2012.

[25] R. S. Berkof, “The input torque in linkages,” *Mechanism and Machine Theory*, vol. 14, no. 1, pp. 61–73, 1979.

[26] V. Van Der Wijk and J. L. Herder, “Synthesis of dynamically balanced mechanisms by using counter-rotary countermass balanced double pendula,” *Journal of Mechanical Design, Transactions of the ASME*, vol. 131, no. 11, pp. 1 110 031–1 110 038, 2009.

NOMENCLATURE

$(.)^*$	Balancing element
μ	Mass per unit length
θ_i	Angle of ith element
E	Material elasticity modulus
G	Material shear modulus
I	Mass moment of inertia
I^{red}	Reduced mass moment inertia
J_{zz}	Second moment of area
k	Transmission ratio
l_i	Length of ith element
m_i	Mass of ith element
r_i	CoM of ith element
t_i	Thickness of element

VII. APPENDIX

A. Beam elements

For the reference mechanism shown in Fig. 2, the first rotational unconstrained natural frequency and the dependence on beam elements is researched. Resulting in 15 where the first natural frequency and error to the converged first natural frequency is plotted. With 2 elements the error is already below 1% and with 3 elements the error is below 0.1%.

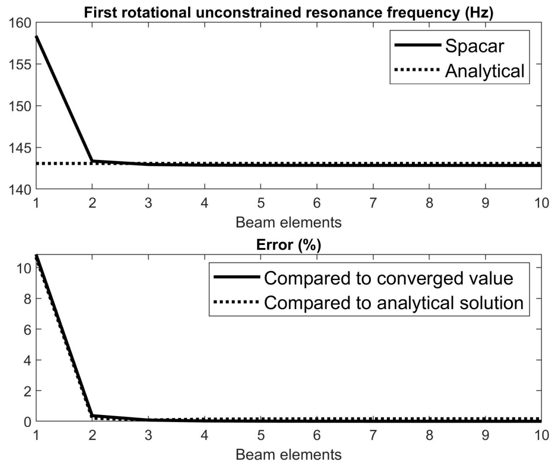

Fig. 15: Error development in number of beam elements

B. Kinematics of inverted four-bar linkage

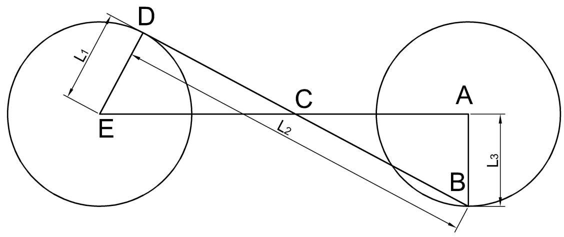

Fig. 16: Geometry of an inherent balanced linkage

The mechanism shown in Fig. 6 is an anti-parallelogram (see Fig. 16). When the positions of E, D, and A are known the position of B can be calculated by drawing a circle with midpoint D and radius L_2. This circle can described by Equation, 16 which represents the possible positions of coupler link when it is only attached to point D.

$$(x - D_x)^2 + (y - D_y)^2 = L_2^2 \tag{16}$$

All the positions of link AB when it is not attached to the coupler link can be described by drawing a circle around point A with radius L_3. This circle can be described by Equation 17.

$$(x - A_x)^2 + (y - A_y)^2 = L_3^2 \tag{17}$$

By calculating the intersection point of Equation 16 and 17, results in two possible solutions for point B. These two solutions represent two assembly modes; parallel and anti-parallel. By checking which point corresponds with which assembly mode results in the solutions for the position of B.

C. Reduced inertia of an inverted four-bar linkage

The reduced inertia is derived from the kinetic energy in the mechanism. The kinetic energy of a four-bar linkage is shown in Equation 18, which is derived by Berkof [25].

$$T = -\frac{1}{2}(K_1\dot{\theta}_1{}^2 + K_2\dot{\theta}_2{}^2 + K_3\dot{\theta}_3{}^2) \tag{18}$$

Where:

$$\begin{aligned} K_1 &= -I_1 - m_1(r_1^2 + l_1 r_1) \\ K_2 &= -I_2 - m_2(r_2^2 - l_2 r_2) \\ K_3 &= -I_3 - m_3(r_3^2 + l_3 r_3) \end{aligned} \tag{19}$$

By rewriting Equation 18 to use the transmission ratios of Equation 14 results in Equation 20.

$$T = \frac{1}{2}(K_1 + K_2 k_2^2 + K_3 k_3^2)\dot{\theta}_1{}^2 \tag{20}$$

The kinetic energy of a rotating object can also be written as in Equation 21.

$$T = \frac{1}{2} I_\theta^{red} \dot{\theta}_i{}^2 \tag{21}$$

Combining and rearranging Equation 20 and 21 results in Equation 22.

$$I_\theta^{red} = K_1 + K_2 k_2^2 + K_3 k_3^2 \tag{22}$$

4

Design and experimental evaluation of a dynamically balanced planar mechanism based on an inverted four-bar linkage aimed at high acceleration applications

Design and experimental evaluation of a dynamically balanced planar mechanism based on an inverted four-bar linkage aimed at high acceleration applications

M.J.J Zomerdijk, V. van der Wijk

***Abstract*—Industrial robotic manipulators in pick-and-place applications require short settling times to achieve high productivity. A manipulator with dynamic unbalance will induce fluctuating reaction forces and moment causing vibrations in the base, which increases settling time and reduces precision. Dynamic balancing eliminates the source of these vibrations with, in general, the addition of counter-masses and counter-inertias. These elements increase moving mass which reduces natural frequencies and therefore results in lower controllability. In order to achieve short settling times, it is therefore key to maximize natural frequencies of the balanced mechanism. To achieve optimal controllability an inverted four-bar linkage architecture is favoured over architectures which depend on counter-rotating flywheels, because they have higher natural frequencies. The goal of this paper is to present and experimentally verify a design approach based on a dynamically balanced inverted four-bar linkage aimed at high acceleration applications. Robustness and dynamical properties are both verified with simulations and in experiments. Experiments show when fully balanced a reduction of 99.3% in reaction forces and 97.8% in reaction moments compared to the unbalanced mechanism. Measurements show the first natural frequency is 212 Hz. Most critical in the design are the stiffness of the first and second link, although the stiffness of the base also has a large impact. Transverse tip accelerations over 21 G are achieved with the balanced prototype. The results of the experiments show that a balanced inverted four-bar linkage architecture can successfully be used in the design of balanced manipulators in high acceleration applications.**

I. Introduction

To stay competitive in industry it is required to reduce production costs and therefore to increase production rates. For robotic manipulators in pick-and-place applications this means more cycles per unit time are required. Settling time has a significant influence on the cycle time and therefore on how many cycles per unit time can be achieved. Settling time is defined as the time to reach and stay within a certain error band of the final position after a motion is initiated. Improving settling time requires to improve acceleration capabilities and controllability. Multiple design approaches exist to achieve optimal settling time in multiple degree of freedom (DoF) manipulators [1]–[3]. These approaches all focus on the manipulator and assume the base rigid. In reality the base is elastic and vibrations in the base affect precision and settling time significantly [4]. In addition, these vibrations can also induce vibrations in other machinery. Removing the source of base vibrations requires to remove fluctuating reaction forces and moments, which can be achieved with dynamic balancing. In fact balancing will result in a dynamic decoupling between the mechanism and the base, which eliminates the need for force frames and vibration isolation [5]. A manipulator is dynamically balanced when both sums of linear and angular momentum stay constant during applicable motions. Although balancing minimizes base vibrations, it will add mass to the mechanism, which degenerates dynamical properties and natural frequencies [6], [7]. To reduce the impact on dynamics and controllability a integral design approach is required.

Literature on dynamic balancing is predominantly theoretical and a significant amount of experiments do not take dynamic properties into account [8]–[10]. Experimentally verified high speed dynamically balanced planar manipulators are the DUAL V and Hummingbird manipulator. The DUAL V manipulator relies on actuation redundancy and is based on a duplicate pantograph architecture. Accelerations over 10 G are reached during movement (17 cm motion distance) [11]. The Hummingbird is a force balanced manipulator with a reaction wheel to achieve dynamic balance, this approach is also known as active balancing. Accelerations up to 50 G are achieved (5 mm motion distance) [12] and the first natural frequency of the mechanism is 1.3 kHz. Active balancing in the Hummingbird only results in a 90% reduction in reaction moments due to non-ideal actuators and friction. Accelerations up to 10 G are reported on a larger scale (25 cm motion distance) with a comparable architecture to the Hummingbird [13], [14].

The goal of this paper is to present and experimentally verify a design approach based on a dynamically balanced inverted four-bar linkage aimed at high acceleration applications. The dynamically balanced inverted four-bar linkage (Fig. 1 and balancing equations of this mechanism are discovered by Ricard and Gosselin [15]. This linkage is an inherent balanced architecture, which have better controllability than counter-rotating flywheel (CRF) based architectures [16]. Better controllability is a result of higher natural frequencies. The design is based on a single rotatable link (single pendulum) (Fig. 1), which can be regarded as one of the building blocks in manipulator design. For instance, a Delta robot [17] is composed of three parallel dyads (double pendulums). The PAR4 [18] robot has four parallel dyads. The IRSbot2 [1]

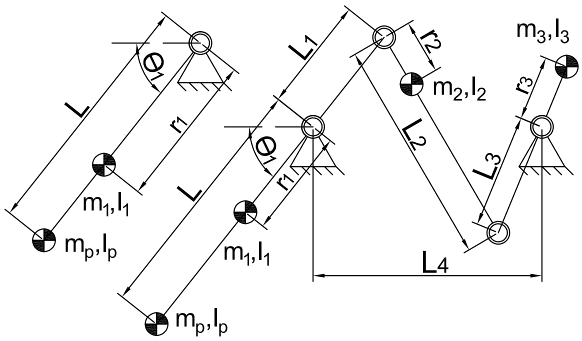

Fig. 1: Unbalanced rotatable link in the upper left corner including parameter definitions. The dynamically balanced inverted four-bar with the unbalanced rotatable link incorporated is on the right including parameter definitions (adapted from [15]).

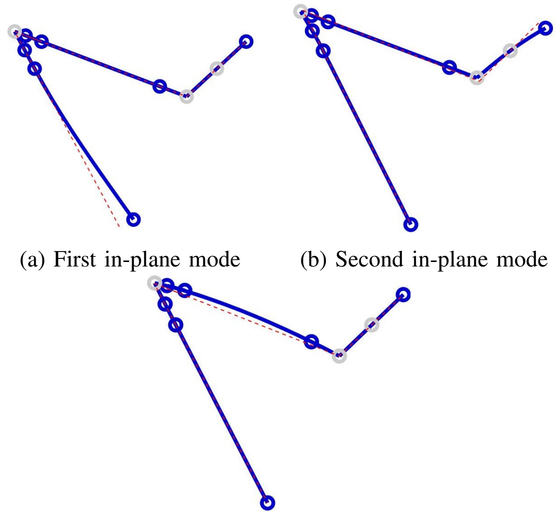

(a) First in-plane mode (b) Second in-plane mode

(c) Third in-plane mode

Fig. 2: In-plane mode shapes in a balanced inverted four-bar mechanism.

is a planar mechanism based on six links connected to each other with revolute joints (6-R six-bar). After the design of the balanced inverted four-bar linkage, robustness and dynamical properties are reviewed. A prototype was built to verify the design experimentally.

In section II the architecture of the mechanism is presented. Section III shows the design of the mechanism and investigates the natural frequencies. In section IV the robustness of the designed mechanism is reviewed. Experimental setup and results are presented in section V and VI. Discussion is located in section VII. Finally, conclusions are provided in section VIII.

II. Mechanism

A. Architecture

Comparative analysis showed that a balanced inverted four-bar linkage architecture should be favoured over CRF based mechanisms when optimal controllability is required [16]. This is a result of higher natural frequencies. The inverted four-bar linkage (Fig. 1) is discovered by Ricard and Gosselin [15] and the design is based on this architecture. The rotatable link is integrated in the inverted four-bar linkage to achieve a dynamically balanced mechanism.

In Fig. 1 the mass, mass moment of inertia (will be referred to as inertia), and centre of mass (CoM) of each link are denoted with m_i ,I_i and r_i, respectively. Subscript $_i$ denotes the link number, which corresponds with Fig. 1. The initial unbalanced rotatable link, which is shown in the upper left corner of Fig. 1, has length L with tip mass m_p and tip inertia I_p. Inertial properties of the tip are included in parameters m_1, r_1, and I_1. The position of the link with respect to the horizontal axis is denoted with θ_1.

The unbalanced mechanism is incorporated in the inverted four-bar linkage on the right of Fig. 1. Parameters introduced for the unbalanced mechanism are also used in the balanced mechanism. Length of the first link in the balanced mechanism is the sum of L and L_1. The distance between the two based attached revolute joints is denoted with L_4. To achieve dynamic balance both Equation 1 and 2 need to be satisfied [15]. Parameters in Equation 1 and 2 correspond with Fig. 1. In addition to the balancing equations, the CoM of each link needs to be on the centre line of the link (as shown in Fig. 1).

Force balance:

$$r_2 = L_2(1 - \frac{m_1 r_1}{m_2 L_1}), \quad r_3 = \frac{m_2 r_2 L_3}{m_3 L_2} \tag{1}$$

Moment balance:

$$\begin{gathered} L_1 = L_3, \quad L_2 = L_4, \\ I_2 = m_2(L_2 r_2 - r_2^2) - I_{c1}, \\ I_3 = -m_3(L_3 r_3 + r_3^2) + I_{c1}, \\ I_{c1} = I_1 + m_1(r_1^2 + r_1 L_1) \end{gathered} \tag{2}$$

B. Natural frequencies

The cross section of each link is a trade-off between mass and stiffness. Optimizing natural frequencies requires insight where additional stiffness is required, mode shapes will help identify these locations. Three distinctive in-plane mode shapes (Fig. 2) can be recognized in the inherent balanced mechanism in Fig. 1.

Mode shapes are determined with Spacar [19]. The first mode shown in Fig. 2a is present in the unbalanced rotatable link as well as the inverter four-bar linkage. The mode shapes shown in Fig. 2b and 2c are only present in the inverted four-bar linkage. The second mode shape (Fig. 2b) is a result of elasticity in link 3 and link 1. The third mode shape (Fig. 2c) is a result of elasticity in link 2. Increasing stiffness in link 3 and along the length of L_1 will increase the natural frequency associated with the second mode shape. Also reducing length L_1 will increase this specific natural frequency, but reduces the

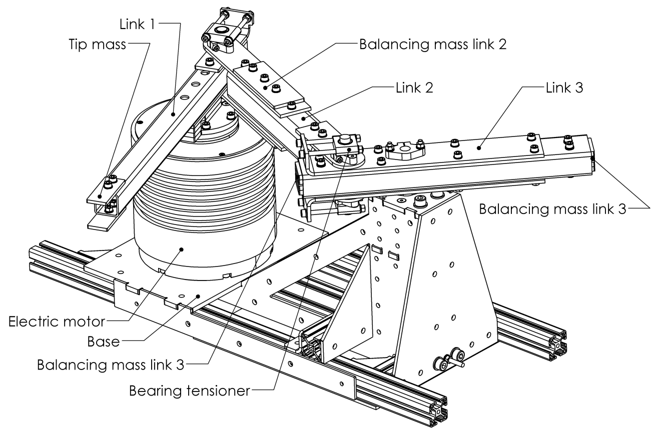

Fig. 3: Final design of the balanced mechanism mounted to the electric motor and the base. The base can be mounted to the machine frame in practical applications.

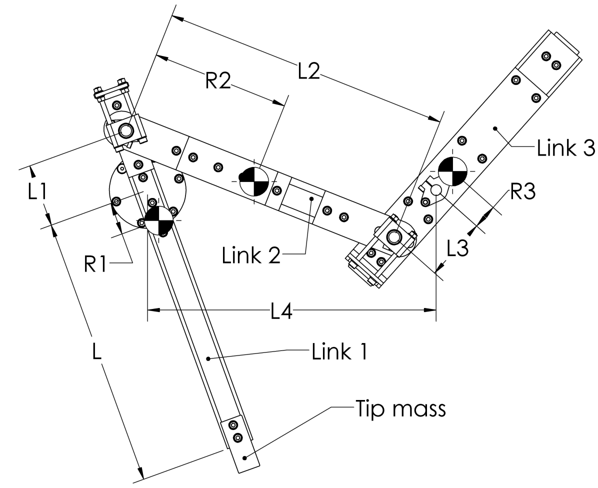

Fig. 4: Top view of the balanced mechanism with the geometric parameters

natural frequency associated with the third mode shape. This is a result of the inverse linear dependency between the mass of the second link (m_2) and length L_1 in Equation 1. Therefore reducing length L_1 will increase mass m_2. Reducing the length of the second link (L_2) will increase natural frequencies associated with the third mode shape, but is subjected to a lower limit. Otherwise the inertia of the second link (I_2) is too low and the balance equations become unsolvable.

The natural frequency associated with the second in-plane mode shape (Fig. 2b) depends on the position of the mechanism. When θ_1 is larger than $90\,\mathrm{deg}$ the excitation of the second mode shape loads link 1 and link 3 predominantly longitudinal. At smaller angles the links will be loaded predominantly transverse. In transverse direction the links have a lower stiffness which results in lower natural frequencies.

III. Design

The dynamically balanced design, including the base, is shown in Fig. 3. In order to reduce mass and costs, plain bearing are used in hinge joints. In addition, the monolithic construction of plain bearings is beneficial for the moment balance quality, because the angular velocity in the whole bearing is constant. In contrast, ball bearing have multiple angular velocities. Each axle has two main bearings and two bearing tensioners. A bearing tensioners is an additional bearing which can be tensioned by bolts to remove play in the main bearings. Friction forces in plain bearings create internal forces, therefore they do not affect the balance quality. An ETEL RTMBi140-100 direct drive motor is used for actuation, in the motor are ball bearings used due to the construction of the motor.

The initial unbalanced mechanism (Fig. 1) has a tip mass (m_p) of 112.12 g, which is connected to the electric motor with a $L = 0.3$ m long link.

Table 1: Parameters of the tubes in the final design

	Link 1	Link 2	Link 3
Outer dimensions (mm)	30x30	40x40	50x30
Wall thickness (mm)	2	4	2

A. Mechanism design

To simplify manufacturing all links will be made from tubes of which the dimensions are listed in Table 1. Additional elements, such as balancing masses and bearing mountings, will be made from sheet metal. All components in the mechanism, except the bearings, axles, and axle mounts, are made from stainless steel (AISI 304). Axles attached to the coupler link and all axle mounts are made from aluminium. The axle between the third link and the base is made from steel.

The top view of the balanced mechanism with geometric design parameters is shown in Figure 4, corresponding inertial and geometric parameters are listed in Table 2. Link parameters m_i,r_i, and I_i include counter-masses and tip mass. Individual counter-masses are denoted with an asterisk, tip mass is denoted with subscript p. Inertia of the links is taken at the link CoM. Due to collisions, the admissible range of motion is from $\theta_1 = 60$ deg till $\theta_1 = 110$ deg.

The parameters in Table 2 are established as a result of an iterative design process based on 3 steps: 1) initial parameters

Table 2: Parameter values of the final design

$[mm]$	$[g]$	$[mm]$	$[kgm^2]$
$L = 300$	$m_p = 112.12$	$r_p = 300.00$	$I_p = 0.0000377$
$L_1 = 70$	$m_1 = 2140.93$	$r_1 = 36.26$	$I_1 = 0.0262$
$L_2 = 320$	$m_2 = 2139.95$	$r_2 = 154.16$	$I_2 = 0.0169$
$L_3 = 70$	$m_3 = 2539.59$	$r_3 = 28.17$	$I_3 = 0.0319$
$L_4 = 320$	$m_2^* = 208.04$	$r_2^* = 124.00$	$I_2^* = 0.000140$
	$m_3^* = 536.47$	$r_3^* = 46.00$	$I_3^* = 0.0131$

optimization with Spacar, 2) Detail computer aided design (CAD), and 3) verification of natural frequencies.

Initial lengths of L_1, L_2, L_3, and L_4 are established by optimization of natural frequencies in Spacar. The simulation in Spacar uses beam elements to model the tubes in Table 1. Mass and inertia of balancing masses and joints are incorporated in the model. Optimization without dimensional constraints on the balancing masses results in initial lengths for L_1, L_2, L_3, and L_4 of 78 mm, 310 mm, 78 mm, and 310 mm, respectively. The second in-plane natural frequency is in that case 565 Hz, which can be assumed as the theoretical maximum of the design.

Final parameters in Table 2 are a trade off between natural frequencies, balancing conditions, geometric constraints, and mass. Satisfying the balancing conditions of the second link may require to alter the length of L_1. The CoM of the second link (r_2) has a large effect on the inertia and mass of the link, which can be seen in Fig. 5. Increasing r_2 exponentially increases the required mass, because high moving mass is undesirable the CoM is therefore subjected to an upper limit. The CoM is also subjected to a lower limit, otherwise the inertia of the link becomes negative. Altering the length of L_1 allows to change the mass and inertia while keeping the CoM of the second link between the upper and lower limit. In the prototype the length of L_1 is reduced to 70 mm to satisfy the balancing conditions. In order to reduce mass in the third link (m_3) may require to increase the inertia (I_3). This is a result of the dependency between mass and inertia in Equation 2. As described by the parallel axis theorem; to increase the inertia, without altering the mass, requires to move the mass further away. This can be achieved by splitting the single balancing mass into multiple distal masses. To keep r_3 constant requires the distal masses to be arrange in a circular pattern with equal spacing. In addition, the inertial properties of all distal masses need to be equal. In the prototype the balancing mass is split in two, which reduces the mass of the third link by 36%. In addition, the second in-plane natural frequency is increased by 5%.

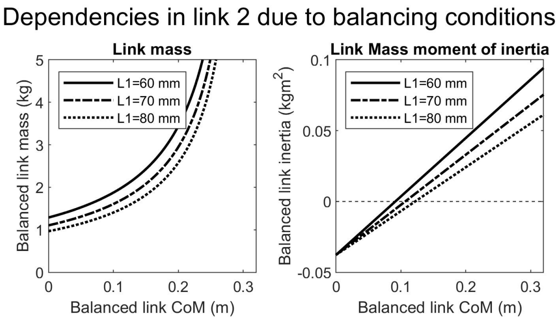

Fig. 5: Dependency in link 2 in the proposed design between mass, inertia and CoM. Figure on the left shows the exponentially increasing required mass to achieve balance with the position of CoM. To reduce mass, the position of the CoM is therefore subjected to an upper limit. Figure on the right shows the required link mass moment of inertia to achieve balance based on the position of the CoM. The position of the CoM is subjected to a lower limit because the balanced link mass moment of inertia can not become negative.

B. Finite elements simulation

The natural frequencies of the CAD model are analysed with the help of Comsol [20]. To speed up the analysis, a simplified model is used which only focusses on the mechanism. Stiffness of bolted connections is not taken into account. Axles and the bearing tensioners are added in the simulation as point masses. Chosen is to perform calculations at $\theta_1 = 88.2$ deg, because the frequency sweep in the experiment will be conducted at the same position. The position in the experiment is chosen to avoid collisions during the frequency sweep. The three distinctive mode shapes in Figure 2 are visible in the simulation results shown in Figure 6.

The natural frequency of the third in-plane mode shape (Fig. 6c) is significantly higher than the second in-plane mode shape (Fig. 6b). Increasing the natural frequency of the second in-plane mode shape requires to add stiffness along the length L_1. Due to the fact that the prototype is structurally based on tubes, adding stiffness in this section is challenging. Although the third in-plane mode

When the angle of θ is reduced to 60 degrees, the natural frequency associated with the second in-plane mode shape drops to 346 Hz. This drop is a result of increased transverse loading of link 1 when this mode is excited. Increasing angle θ to 115 degrees results in a natural frequency of 390 Hz, due to increased longitudinal loading. Other mode shapes in Fig. 6 and 7 are marginally affected by the position of the mechanism.

In addition to the in-plane modes shapes, three out-of-plane modes are of interest. First out-of-plane mode (Fig. 7a) is also present in the unbalanced mechanism. The second mode is a result of the balancing mass added at the end of the third link (Fig. 7b). The natural frequency associated with this mode shape is more than twice the first natural frequency. The third out-of-plane mode shape (Fig. 7c) will have the largest effect on the controllability because longitudinal loading of link 2 occurs during motion which excites this mode. Excitation of the other two out-of-plane mode shapes is significantly lower during motion, because actuation will not exert out-of-plane loads on link 1 and 3.

IV. Robustness and manufacturing tolerances

The influence of mass errors in counter-masses, length errors in links, and payload deviations on the balance quality will be studied. Tolerances in manufacturing and material properties will cause mass errors. To minimize mass errors all elements will be weighed with an accuracy of 0.01 g and measurements will be incorporated in the CAD model before calculation of the balancing masses. Assumed is that mass errors will not affect the mass distribution and radius of gyration, which makes mass and inertia errors linearly dependent. Length errors are assumed to not influence the link

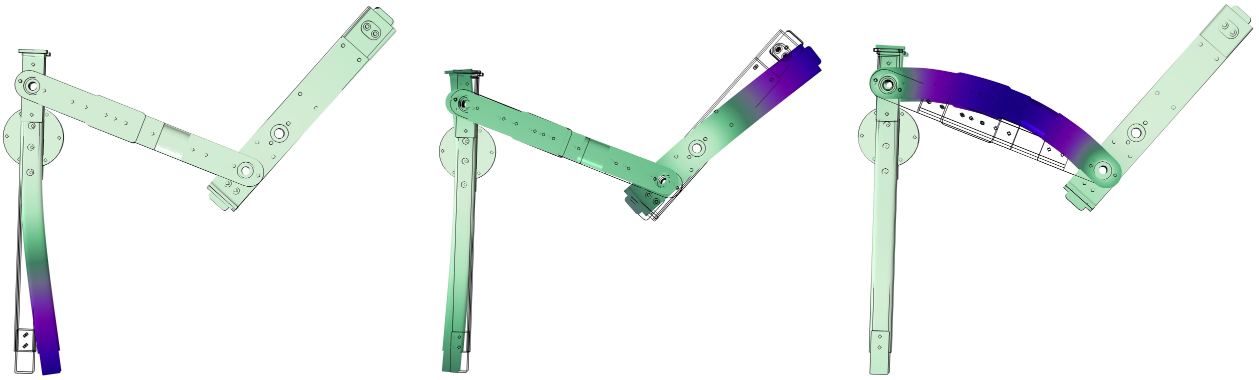

(a) First in-plane mode at 312 Hz (b) Second in-plane mode at 353 Hz (c) Third in-plane mode at 826 Hz

Fig. 6: In-plane mode shapes in finite element analysis at $\theta_1 = 88.2$ deg, showing in dark blue where the largest displacements occur due to the excitation of a specific mode shape

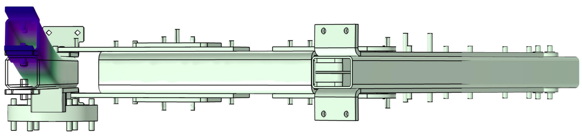

(a) First out-of-plane mode at 324 Hz

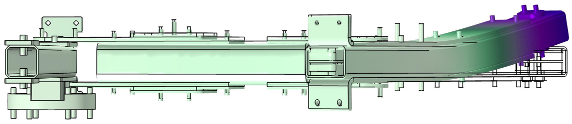

(b) Second out-of-plane mode at 696 Hz

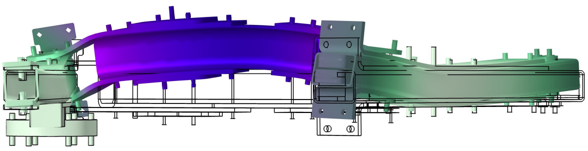

(c) Third out-of-plane mode at 721 Hz

Fig. 7: Out-of-plane mode shapes in finite element analysis at $\theta_1 = 88.2$ deg, showing in dark blue where the largest displacements occur due to the excitation of a specific mode shape.

Table 3: Parameters of the unbalanced rotatable link including the inertia of the electric motor

$[g]$	$[mm]$	$[kgm^2]$
$m_u = 1719.16$	$r_u = 64.75$	$I_u = 0.0222$

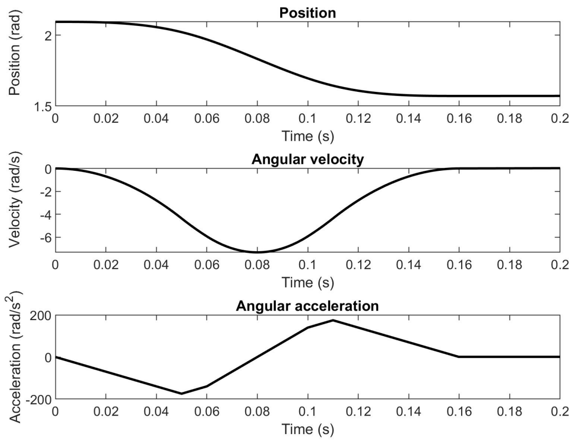

Fig. 8: Reference trajectory based on S-curve profile which moves the mechanism from $\theta_1 = 98.2$ deg to $\theta_1 = 68.2$ with a peak rotational acceleration of 174.5 rad/s^2

mass. The balance quality is defined as a percentage, where 100% means all shaking forces and moments are removed, while 0% means they are equal to the unbalanced mechanism. The parameters of the unbalanced mechanism, including the electric motor, are shown in Table 3. Analysis is performed in Simulink [21] with an ODE45 solver. Control performance is omitted by inputting the motions directly. Force balance quality is determined by the peak reaction force, calculated with max($\sqrt{F_x^2 + F_y^2}$). Moment balance quality is calculated with max(M_z). Reference trajectory is based on a S-curve profile (shown in Fig. 8) and is equal to the profile in the experiment.

A. *Mass errors*

The consequence of errors in the counter-masses is shown in Fig. 9. As can be seen in Fig. 9, the third link is more sensitive to balancing mass errors than the second link. Force balance quality can be further improved by compensating errors in $M2_{cm}$ in $M3_{cm}$, due to the fact that force balance conditions of link 3 are dependent on link 2 (Equation 1).

Errors in $M3_{cm}$ have significantly larger influence on the moment balance quality, because the third link is more important for the moment balance. To achieve moment balance a constant angular momentum of the whole mechanism is

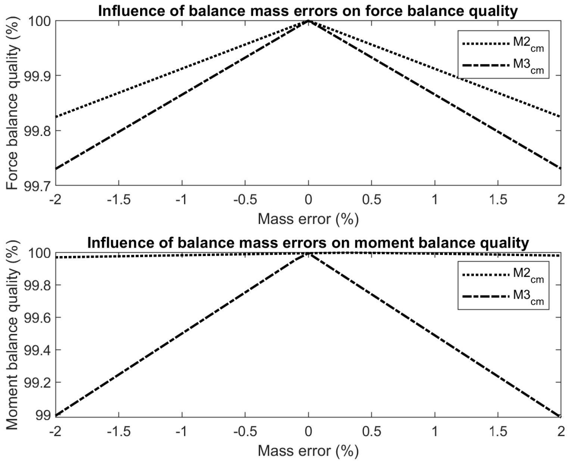

Fig. 9: Influence of mass errors in balancing masses on balance quality. The balance quality indicates the reduction in reaction forces and reaction moments compared to the unbalanced mechanism

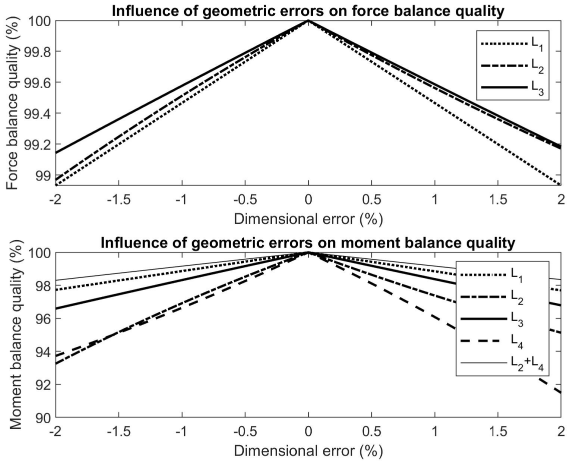

Fig. 10: Influence of geometric errors on balance quality. The balance quality indicates the reduction in reaction forces and reaction moments compared to the unbalanced mechanism

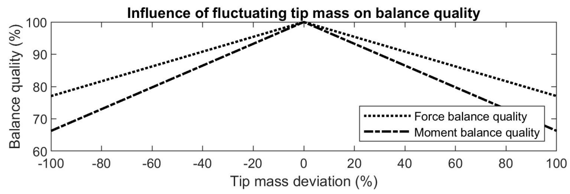

Fig. 11: Influence of payload deviations on balance quality. The balance quality indicates the reduction in reaction forces and reaction moments compared to the unbalanced mechanism

required [6]. The total angular momentum of a four-bar linkage is dependent on the inertia and angular velocity of each link [22]. The total angular momentum is constant because the second and third link compensate the inertia and angular velocity of the first link. The third link is more important to moment balance because it has a higher inertia and angular velocity during admissible motions than the second link. The higher angular velocity during admissible motions is a result of a higher transmission ratio between the first and third link compared to the transmission ratio between the first and second link.

The counter-masses will be laser cut, over multiple test pieces the average raw mass error is 0.61%. With post-processing the mass error will even be lower. Within the specified mass tolerances the influence of mass errors on the balancing quality is marginal.

B. Geometry errors

Figure 10 shows the influence of length errors on the balance quality. As can be seen the balance quality is more sensitive to geometric errors than mass errors. The moment balance quality is most sensitive to errors in L_4 because they also affect the torque arm between the two revolute joints attached to the base. Sensitivity to errors in L_2 and L_4 can be reduced by assuring that those lengths are equal.

Length errors due to production tolerances are estimated to be below 0.1 mm. Although a tensioning device is added to remove play in the plain bearings, they can still introduce an error of up to 0.05 mm at each bearing. Geometric errors could therefore be up to 0.2 mm in L_2 and L_3 and up to 0.15 mm in L_1. Within these tolerances it is estimated that the force balance quality is above 99% and the moment balance quality above 98%.

C. Fluctuating tip masses

In applications with fluctuating tip masses, the balance conditions are not satisfied during the whole cycle. As can be seen in Fig. 11, the balance quality is lower when the tip mass is reduced. When the tip mass $m_p = 112.12$ g is completely removed, the force balance quality reduces to 75% and the moment balance quality to 65%.

D. Bearing loads and actuation torques

The addition of mass caused by balancing will increase bearing loads and actuation torques. The actuation torque is 2.2 times higher for the balanced mechanism compared to the unbalanced case. Comparable results are seen in earlier research [16], where the reduced inertia is 2-3 times higher in the balanced mechanism. The reduced inertia is an indicator for required actuation torque. The peak loads in the bearings mounted at the base are 4.2 times higher in the balanced mechanism.

V. Experimental setup

Reaction forces and moments will be measured by 3 single point load cells, each connected to a Penko SGM 720 load cell transducer. The load cells can individually measure a maximum force of 49 N with a precision of 0.05%, sampling frequency is 1 kHz. The locations of the load cells are shown in Figure 12, positions are denoted with numerical balloons. Load cell 1 will measure forces on the X-axis, load cell 2 and 3 measure forces on the Y-axis. Moments around the Z-axis are calculated by multiplying the force measured at load cell 3 with the distance between load cell 2 and 3. The base is suspended by chains to unload the load cells from the gravity and allow small movements in the XY-plane. To minimize transverse forces, load cells which measure forces on the Y-axis are attached with a 0.5 mm rod to the base (Detail A in Fig. 12). The load cell which measures forces on the X-axis is attached to the base with a 1 mm rod.

Identification to determine the natural frequencies of the system is conducted with the ETEL AccurET 400 motor controller. Balance quality is measured by executing the reference trajectory shown in Fig. 8, motions are executed by feedback control only. The feedback control is automatically tuned by the ETEL motion controller. The ETEL RTMBi140-100 direct drive motor can deliver a peak torque of 131 Nm. The base and measurement frame are structurally made from aluminium extrusion profiles which are stiffened with AISI 304 stainless steel plates. The experimental setup of the prototype is shown in Fig. 13.

VI. Experimental results

Four experiments are conducted: 1) balance quality when dynamically balanced, 2) balance quality with half of the tip mass (regarded as partly balanced), 3) identification of natural frequencies, and 4) maximal acceleration capabilities of the prototype. Balance quality is determined in the same way as the robustness analysis, the simulated values of unbalanced mechanisms are used in the calculation. The simulation is chosen as reference because results of the robustness analysis stay applicable. The results of the unbalanced mechanism when execution the motion profile in Fig. 8 are shown in Fig. 14.

The measured reaction forces and moments are compared to the simulation, which is based on the CAD model with weighed parts. The motion profile for both the simulation and experiment is shown in Fig. 8, total motion time is 160 ms. Converting the peak rotational acceleration of 174.5 rad/s^2 in Fig. 8 to a transverse tip acceleration results in an acceleration of 51.1 m/s^2 or 5.2 G. Both simulation results and measurements of reaction forces and reaction moments of the balanced mechanism are shown in Fig. 15.

As can be seen in Fig. 15, the measured reaction forces and moments are higher than simulated. Due to damping in the system the measurements are smoother than the simulated. Based on the measurement data, the force and moment balance quality during motion are 99.3% and 97.8%, respectively. Both values are close to expected values of the robustness analysis. The moment balance quality is slightly lower than expected, this could be caused by an error in the reported motor inertia of the manufacturer. In addition, the third link is slightly curved and has a not completely rectangular cross-section, which also results in an error. Vibrations in the measured values are noticeable after the motion is finished, which increase the measured forces significantly after the motion is finished. These values are therefore omitted in determining the balance quality.

Robustness is measured by removing half of the tip mass at the end of the first link. The mass m_p equals in this case 56.06 g. Measurements are conducted based on the motion profile in Fig. 8. Results of both the simulation and experiment are shown in Fig. 16.

As can be seen in Fig. 16 the reaction forces and reaction moments are in the measurements much lower than in the simulation. This is caused by the transverse stiffness of the connection rods between the load cells and the base. More load on the load cells require more bending of the connection rods and therefore larger errors. To solve this issue, the accelerations in the motion profile will be reduced such that the peak reaction forces and reaction moments are similar to

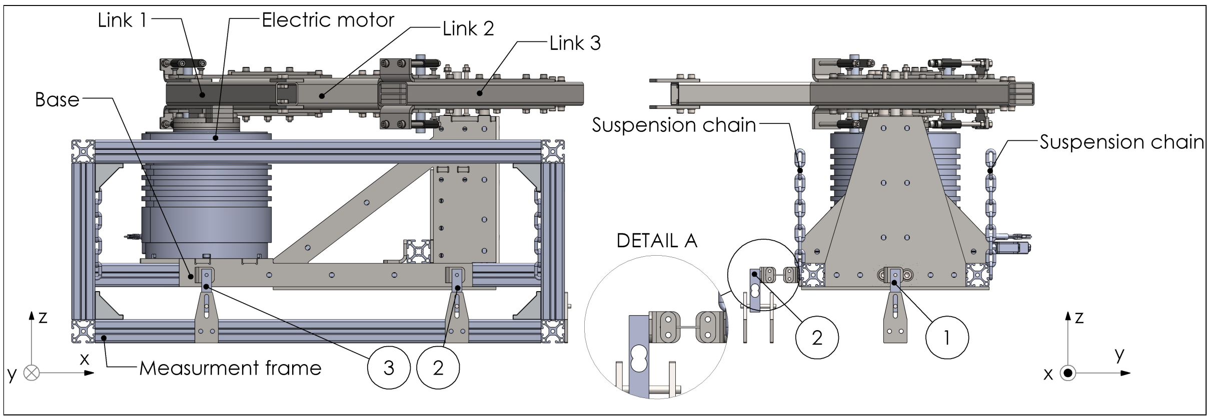

Fig. 12: CAD model of experimental setup with base suspended by chains to remove gravity loads from the measurement setup. Numerical balloons denote the positions of the load cells. In the right figure the measurement frame is hidden. Detail A shows the connection between a load cell and the base.

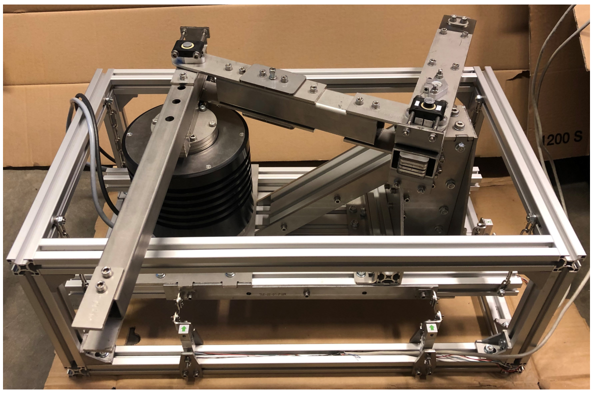

Fig. 13: Experimental setup of the balanced inverted four-bar linkage with the base suspended by chains and mounted to the load cells for force measurements.

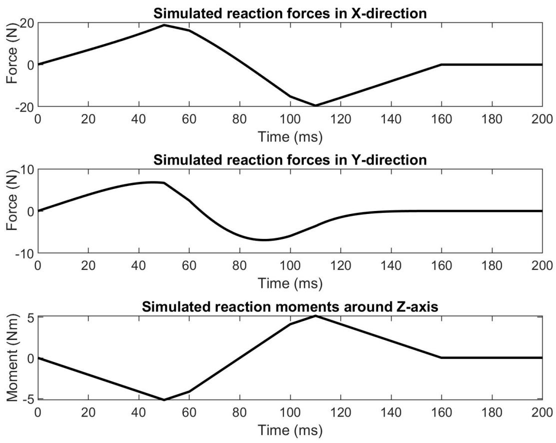

Fig. 14: Simulation of reaction forces and moments of unbalanced mechanism subjected to the motion profile in Fig. 8. During motion the peak reaction force (magnitude of force vector composed out of reaction forces on the X- and Y-axis) is 25.54 N and the peak reaction moment 5.16 Nm.

the results (Fig. 15) of the completely balanced mechanism. This means the peak acceleration is reduced with a factor 10 which results in a peak angular acceleration of 17.45 rad/s^2 and a transverse tip acceleration of 5.11 m/s^2 or 0.52 G. Measurement results are shown in Fig. 17.

As can be seen in Fig. 17, the measurements are close to the simulated values. The reaction forces are slightly lower than simulated which could still be caused by transverse stiffness of the connection rods, but also vibrations in the measurement setup. When the results of the balanced mechanism in Fig. 15 are compared with the results in Fig. 17, it becomes clear there are far more vibrations during motion in the latter. With half the tip mass, measured force and moment balance quality are 90.3 % and 81.9%, respectively. The robustness analysis predicted that the force balance quality should be 85.3% and

Table 4: Observable natural frequencies of the balanced mechanism at $\theta_1 = 88.2$ deg. Comparing both the FEA and measured values.

	f_1	f_2	f_3
FEA	312 Hz	721 Hz	826 Hz
Measurements	212 Hz	443 Hz	637 Hz

moment balance quality 83.12%. With a 10 times higher peak acceleration, the balanced mechanism has comparable reaction forces and reaction moments to the case with reduced tip mass. This shows the performance improvement when the mechanism is completely balanced.

To avoid collisions a frequency sweep of the mechanism is performed at the position $\theta_1 = 88.2$ deg. At this position the values in the FEA will be compared with the measurements, results are shown in Table 4. Raw data of the frequency sweep can be found in the appendix.

As can be seen in Table 4, the first measured resonance is more than 30 % lower than the results in FEA. One explanation for this reduction is the elasticity of the base, which was assumed rigid in the FEA study. Increasing the stiffness of the base with two additional structural members resulted in Table 4, without these additional members the natural frequency f_1 was 14% lower. Further improving the stiffness of the base will therefore result in better coherence between the measurements and FEA. The bolted connection of the first link to the motor also has a lower stiffness than simulated, which further reduces the natural frequencies.

Tip accelerations over 21 G are achieved with the balanced experimental setup. The ETEL motion controller can not directly measure angular acceleration during motion, therefore the angular acceleration is derived from the angular velocity (central finite difference). The motor torque is calculated from the motor current using a motor torque constant of 4.264 Nm/A. Both the angular acceleration and motor torque are compared in Fig. 18.

As can be seen in Fig. 18 the measured angular acceleration is almost equal to the simulation. This confirms the tip has successfully reached a transverse tip acceleration over 21 G, showing the potential for high accelerations. In simulations the peak actuation torque is 46.7 Nm, while in reality 133.2 Nm is measured, which means the actuator is fully saturated. This higher torque is a result of friction in the mechanism and PID control. Higher accelerations can be reached by implementing feedforward control and reducing friction. The actuation torque is not instantly zero after the motion is finished, because the PID is still damping out vibrations in the mechanism. Measurement results of reaction forces and moments during the motion are shown in Fig. 19.

As can be seen in Fig. 19, the highest forces and moments are measured after the motion should be finished. This could be caused by a higher reaction moment which affects measurements. In addition, the elastic behaviour of the mechanism combined with high actuation torques can cause elastic

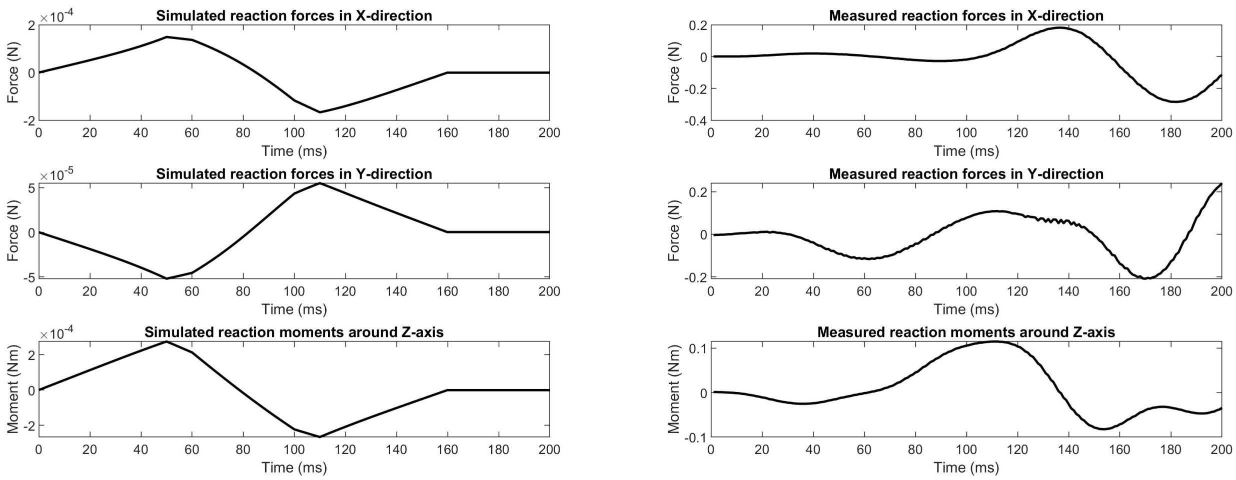

Fig. 15: Comparison between simulated and measured reaction forces and moments of the balanced mechanism, with a maximal tip acceleration of 5.2 G

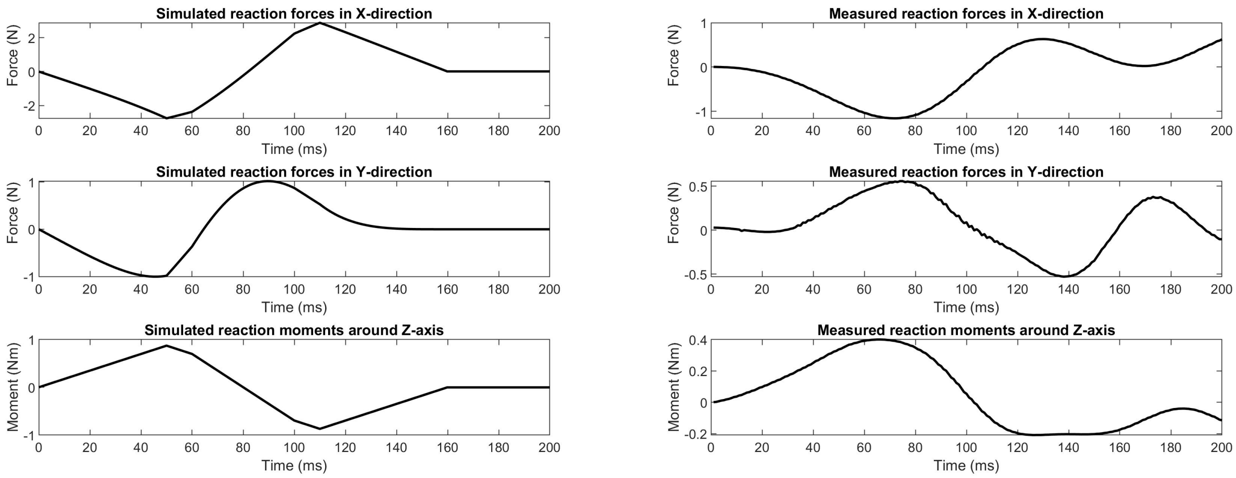

Fig. 16: Comparison between simulated and measured reaction forces and moments of the balanced mechanism with 50% of the designed tip mass, with a maximal tip acceleration of 5.2 G

deformation in the mechanism, which results in unbalance. These measured values result in a force and moment balance quality of 97.2% and 96.9 %, respectively. These values are both lower than the measurements with accelerations of 5 G, which could be an indication that unbalance occurs due to elastic behaviour.

VII. Discussion

This paper presented the design and experimental verification of a dynamically balanced inverted four-bar mechanism. During the design the focus was largely on the mode shapes and natural frequencies, but the significance of each mode is not analysed. Analysis which takes mode participation factors into account can help gain insight how much a mode contributes to the dynamic response when actuated in a particular direction [23]. The added bode plot of the system in the appendix shows that the second resonance peak is higher than the first peak. This means the second peak is limiting the controllability instead of the first peak. If the second resonance peak can moved below the first resonance peak, the controllability will be increased significantly.

The impact of elasticity in the mechanism and base on the reaction forces and reaction moments are not taken into account in the simulations. In reality the vibrations caused by this elasticity will cause unbalance which reduces the balance quality because the mass distribution is affected. Increasing accelerations will result in more accelerations and therefore the balance quality will be lower. Each balancing principle, except duplicate mechanisms, will have this issue [16]. Improving the stiffness of the mechanism results in a lower vibrational amplitude, which reduces disruptions in mass distribution. When the mass distribution is less disrupted the balance quality will be higher.

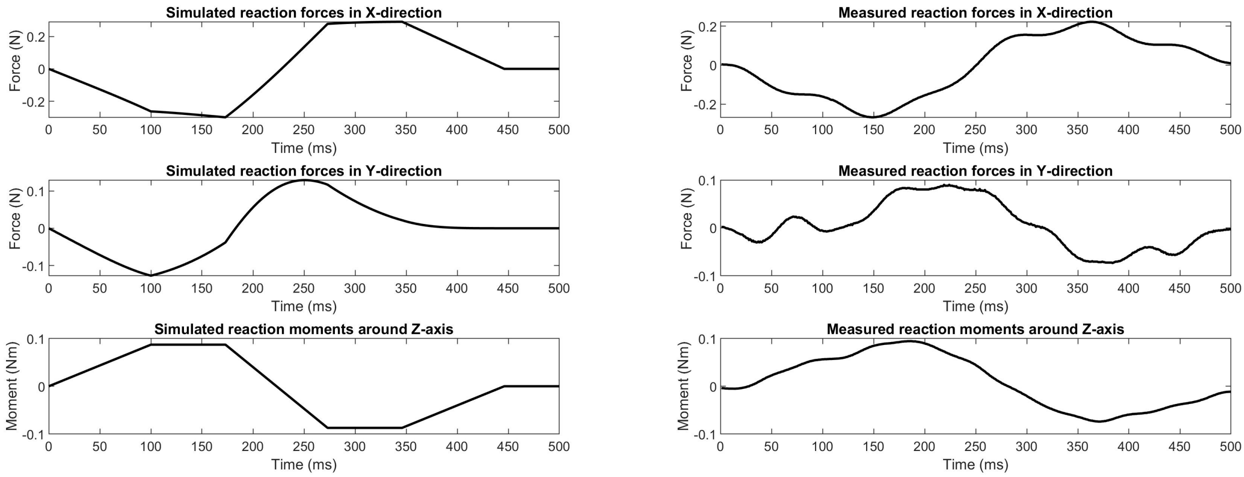

Fig. 17: Comparison between simulated and measured reaction forces and moments of the balanced mechanism with 50% of the designed tip mass, with a maximal tip acceleration of 0.52 G

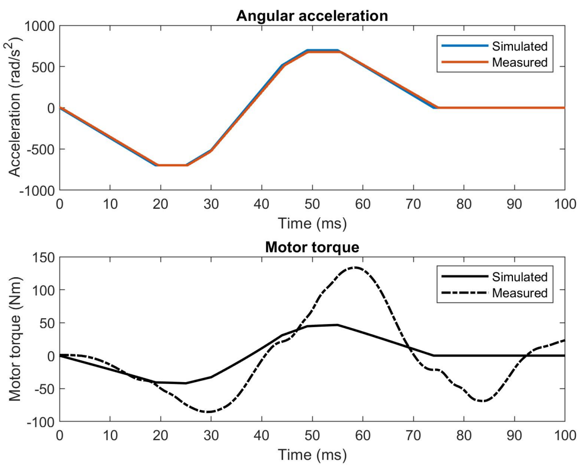

Fig. 18: Comparison of angular acceleration and motor torque between measurements and simulation for a motion which has a peak transverse tip acceleration over 21 G. Motor torque is calculated with a motor torque constant of 4.264 Nm/A.

Usage of stainless steel tubes and sheet metal simplified manufacturing, but caused limitations in the design. In addition, the tubes were not completely straight and square which reduced the balance quality. By CNC milling the parts could have more design freedom and better tolerances. Both of these factors will improve balance quality and controllability. A topology optimization could added to improve controllability even more [24]. The objective of the topology optimization should be maximizing natural frequencies. The balancing conditions need to be added as constraints to the optimization.

Due to the low transverse stiffness of the connection rods between the load cells and the base, combined with the high mass of the base and mechanism, a rotation around the z-axis with a frequency of 18.18 Hz is visible in the results. When stiffer connection rods are used the frequency becomes higher and the vibrations damp out faster. Transverse loading of all connection rods only occurs in a rotation, translations will always load one or more connection rods longitudinal. Longitudinal stiffness of the connection rods is much higher than transverse stiffness. These vibrations disrupt the measurements and result in higher measured forces. Improving the transverse stiffness of the connection rods reduces these vibrations but results in a large error in the measurements. The transverse stiffness of the rods will then cause that measured values are too low. Comparable issues are reported with a measurements setup based on a multi DoF force measurement sensor [11].

The tension mechanism of the plain bearings is difficult to tune. Less tension reduces friction, which reduces the steady state error. A lower steady state error means the integral term of the PID is lower, making the controller less aggressive and reduces fluctuations in actuation torque. Low tension is therefore beneficial for PID control, but low tension also increases the chance of play in the mechanism. Finding an optimum which both removes play and has low friction is challenging. In addition, the control in the prototype relies only on PID, by implementing feedforward control, higher accelerations can be achieved because the PID only needs to focus on error rejection. With this approach less actuation torque is used for tracking and more torque is available for accelerations. The calculation of feedforward torques will require a real time operating system which communicates with the ETEL control system.

VIII. Conclusion

The design and experimental verification of a dynamically balanced single DoF rotatable link were presented in this paper. The main goal of this paper was to present and experimentally verify a design approach based on a dynamically balanced inverted four-bar linkage aimed at high acceleration

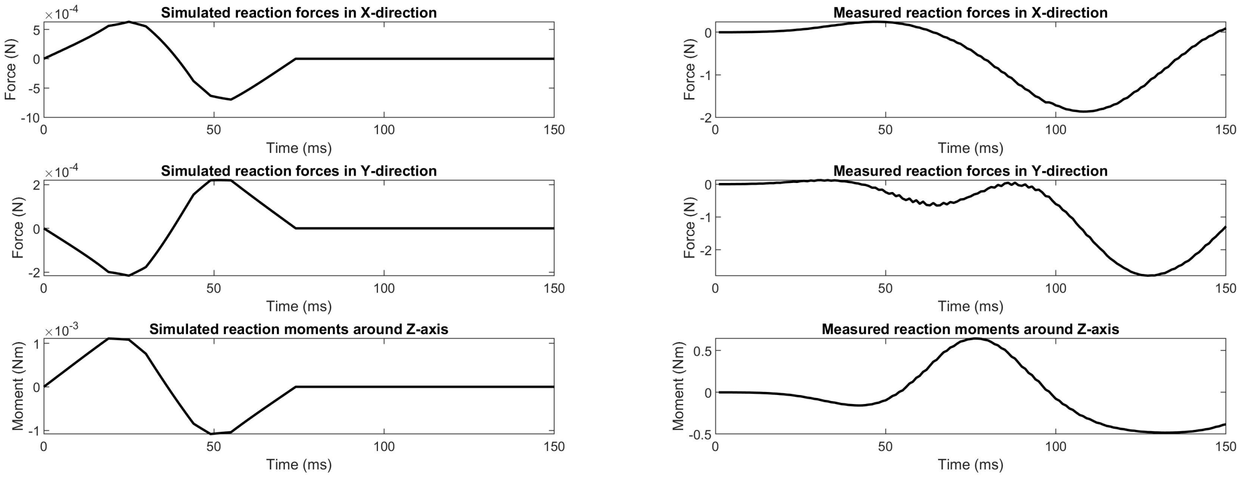

Fig. 19: Comparison between simulated and measured reaction forces and moments of the balanced mechanism, with a maximal tip acceleration over 21 G

applications. A rotatable link was chosen as an initial unbalanced mechanism because this is a building block in the design of robotic manipulators. The inverted four-bar linkage dynamically balances the rotatable link by making it part of the four-bar linkage. The dynamic properties of the mechanism are reviewed by analysing the first three in-plane natural frequencies, showing that the transverse stiffness of the first and second link have considerable influence on the natural frequencies. In terms of balance robustness the mechanism shows more prone to geometric errors than to mass errors. A prototype manipulator was built to verify both dynamic and balanced properties. The prototype successfully performed high accelerations movements with minimal reaction forces and reaction moments. A reduction of 99.3% in reaction forces and 97.8% in reaction moments was measured compared to the unbalanced mechanism. By reducing manufacturing tolerances, even better performance in terms of balancing quality is expected. The performance of the balanced mechanism is compared to a case with half the tip mass (near perfect balance). The balanced mechanism achieved 10 times higher peak accelerations with comparable reaction forces and reaction moments. With half of the designed tip mass mounted, a force and moment balance quality was achieved of 90.3% and 81.9%, respectively. Although these values are lower than the balanced mechanism, reaction forces and moments are still much lower than the unbalanced mechanism. First measured natural frequency of the mechanism is 212 Hz which is lower than simulated in FEA, mainly caused by the lower stiffness of the subframe. The prototype shows that it is possible, even with relative basic production methods, to achieve a dynamically balanced mechanism which can be used in high acceleration applications. With the experimental setup a maximum transverse tip acceleration of 21 G is achieved. This research shows that an inverted four-bar architecture is applicable in practical cases to the building blocks of robotic manipulators. Extending the theory to multiple DoF can therefore result in dynamically balanced manipulators which have short settling time.

References

[1] C. Germain, S. Caro, S. Briot, and P. Wenger, "Optimal design of the IRSBot-2 based on an optimized test trajectory," *Proceedings of the ASME Design Engineering Technical Conference*, vol. 6 A, 2013.

[2] S. Briot, A. Pashkevich, and D. Chablat, "On the optimal design of parallel robots taking into account their deformations and natural frequencies," *Proceedings of the ASME Design Engineering Technical Conference*, vol. 7, no. PARTS A AND B, pp. 367–376, 2009.

[3] F. Pierrot, C. Baradat, V. Nabat, O. Company, S. Krut, and M. Gouttefarde, "Above 40g acceleration for pick-and-place with a new 2-dof PKM," *Proceedings - IEEE International Conference on Robotics and Automation*, vol. 2, pp. 1794–1800, 2009.

[4] V. Arakelian, "Inertia forces and moments balancing in robot manipulators: a review," *Advanced Robotics*, vol. 31, no. 14, pp. 717–726, 2017.

[5] V. van der Wijk, "Methodology for analysis and synthesis of inherently force and moment-balanced mechanisms: theory and applications," Ph.D. dissertation, University of Twente, Enschede, The Netherlands, apr 2014.

[6] V. van der Wijk, J. L. Herder, and B. Demeulenaere, "Comparison of various dynamic balancing principles regarding additional mass and additional inertia," *Journal of Mechanisms and Robotics*, vol. 1, no. 4, pp. 1–9, 2009.

[7] J. J. De Jong, B. E. M. Schaars, and D. M. Brouwer, "The influence of flexibility on the force balance quality: a frequency domain approach," *Proceedings of the 19th international conference of the European Society for Precision Engineering and Nanotechnology*, no. June, pp. 2–5, 2019.

[8] S. Foucault and C. M. Gosselin, "Synthesis, design, and prototyping of a planar three degree-of-freedom reactionless parallel mechanism," *Journal of Mechanical Design, Transactions of the ASME*, vol. 126, no. 6, pp. 992–999, 2004.

[9] T. Laliberté and C. Gosselin, "Synthesis, optimization and experimental validation of reactionless two-DOF parallel mechanisms using counter-mechanisms," *Meccanica*, vol. 51, no. 12, pp. 3211–3225, 2016.

[10] J. de Jong, J. van Dijk, and J. Herder, "A screw based methodology for instantaneous dynamic balance," *Mechanism and Machine Theory*, vol. 141, pp. 267–282, nov 2019.

[11] V. van der Wijk, S. Krut, F. Pierrot, and J. L. Herder, "Design and experimental evaluation of a dynamically balanced redundant planar 4-RRR parallel manipulator," *The International Journal of Robotics Research*, vol. 32, no. 6, pp. 744–759, 2013.

[12] J. Karidis, G. McVicker, J. Pawletko, L. Zai, M. Goldowsky, R. Brown, and R. Comulada, "The Hummingbird minipositioner-providing three-axis motion at 50 g's with low reactions," in *Proceedings 1992 IEEE International Conference on Robotics and Automation*, vol. 1. IEEE Comput. Soc. Press, 1992, pp. 685–692.
[13] H. F. Menschaar, A. B. Ariens, J. L. Herder, and B. M. Bakker, "Five-bar mechanism with dynamic balancing means and method for dynamically balancing a five-bar mechanism," WIPO Patent WO2 006 080 846A1, 2006.
[14] R. Raaijmakers, "Besi zoekt snelheidslimiet pakken en plaatsen op," Sep 2007. [Online]. Available: https://mechatronicamachinebouw.nl/artikel/besi-zoekt-snelheidslimiet-pakken-en-plaatsen-op/
[15] R. Ricard and C. M. Gosselin, "On the Development of Reactionless Parallel Manipulators," *ASME Design Engineering Technical Conferences and Computers and Information in Engineering Conference*, no. September, pp. 1–10, 2000.
[16] M. Zomerdijk, "Controllability of dynamically balanced mechanisms: A comparative analysis," Master's Thesis, TU Delft, 2020.
[17] R. Clavel, "Device for the movement and positioning of an element in space," US Patent US4 976 582A, 1990.
[18] V. Nabat, M. de la O Rodriguez, O. Company, S. Krut, and F. Pierrot, "Par4: very high speed parallel robot for pick-and-place," in *2005 IEEE/RSJ International Conference on Intelligent Robots and Systems*. IEEE, 2005, pp. 553–558.
[19] J. B. Jonker and J. P. Meijaard, "SPACAR — Computer Program for Dynamic Analysis of Flexible Spatial Mechanisms and Manipulators," in *Multibody Systems Handbook*. Berlin, Heidelberg: Springer Berlin Heidelberg, 1990, pp. 123–143.
[20] COMSOL AB, "Comsol multiphysics® 5.4."
[21] Mathworks, "Matlab® r2019a update 9."
[22] R. S. Berkof and G. G. Lowen, "A New Method for Completely Force Balancing Simple Linkages," *Journal of Engineering for Industry*, vol. 91, no. 1, pp. 21–26, feb 1969.
[23] J. H. Park and H. Asada, "Concurrent design optimization of mechanical structure and control for high speed robots," *Journal of Dynamic Systems, Measurement and Control, Transactions of the ASME*, vol. 116, no. 3, pp. 344–356, 1994.
[24] S. Briot and A. Goldsztejn, "Topology optimization of a reactionless four-bar linkage," *Mechanisms and Machine Science*, vol. 50, pp. 414–421, 2018.

IX. Appendix

A. *Frequency response*

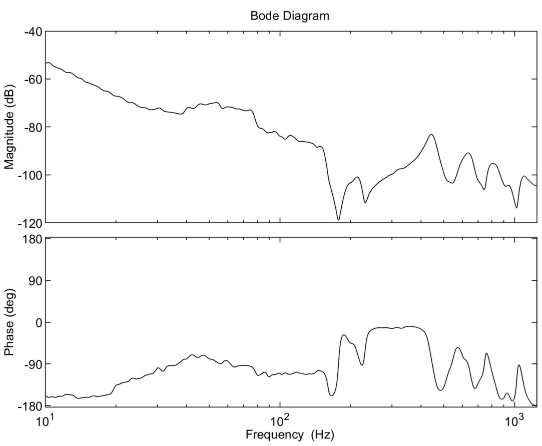

Fig. 20: Bode plot of the balanced mechanical system with motor torque as input and rotary position as output

5
Discussion

In this thesis the application of dynamic balancing in high acceleration mechanisms have been investigated, aiming at reducing the settling time. Various observations during research are discussed in this section.

5.1. Guidelines to reduce settling time

In chapter 2, a set of design principles were derived with the goal to reduce settling time. Chapters 3 and 4 were centred around the principle that balancing eliminates base vibrations and as a result settling time and precision can be improved. It was experimentally shown that practical implementation in a high acceleration application is feasible and has potential. The exact reduction in settling time was not quantified, due to the dependency on a large amount of variables and conditions, as was concluded in chapter 2, which requires a significant amount of assumptions. Instead the settling time was indirectly quantified by parameters which have significant influence, such as natural frequencies and acceleration capabilities. These parameters give a clear indication whether modifications improve settling time or not. In terms of control principles in chapter 2, the research in chapter 3 and 4 was mainly centred around the guideline that improving natural frequencies improves control bandwidth.

In chapter 2, design principles for actuation were formulated. Based on these principles a direct drive was used in the experimental setup. On the other hand, actuation redundancy was also formulated in a design principle, but was not applied due to the increased complexity and additional control. Actuation redundancy can still be applied to the inverted four-bar linkage by adding an additional actuator to the second base attached revolute joint. The effect of actuation redundancy on the design and controllability of the linkage needs to be studied in further research.

Design principles in chapter 2 which were aimed at multiple DoF mechanisms, were not applicable due to the choice of a single link mechanism in chapter 3 and 4. In addition, a significant amount of design principles were not considered due to the high level of complexity.

5.2. Quantification of controllability in balanced mechanisms

Determining the controllability of a balanced mechanism is, in general, more complex than for unbalanced mechanisms. The compared balancing principles in chapter 3 all result in multiple dynamic systems in parallel which, are attached a single actuator. If this actuator is infinitely stiff then these multiple dynamic systems are decoupled from each other. The stiffness of an actuator is in reality virtual and a result of the feedback loop. This virtual stiffness is therefore limited by the bandwidth of the feedback loop, which, in turn, is limited by the natural frequencies of the mechanism. Linearisation in modal analysis is based on the assumption that the joint angle can be perfectly controlled [1], which is also known as perfect tracking. This requires a motor with infinite virtual stiffness resulting in a dynamic decoupling between balancing elements and the initial link. Chosen is therefore to give the actuator zero stiffness, which means the rotary unconstrained natural frequencies are calculated. In addition, the first natural frequency, after the rigid body modes, is the first vibrational frequency of the mechanism, which makes comparison, without visualisation of the mode shapes, more convenient.

During the design in chapter 4 was switched back to modal analysis which assumed perfect tracking. This choice was made because it gave more insight in the mode shapes and verification in experiments was more convenient. The main problem with evaluating natural frequencies is that they give insight in the size of vibrational amplitudes, but they do not indicate how much energy is stored in a frequency. During experiments it was noticed that not the first but the second resonance was limiting controllability. This is caused by more energy storage in the second resonance. A solution to quantify the energy stored in a mode is to analyse the mode participation factors. The mode participation factor shows how much a mode contributes to the dynamic response when actuated in a particular direction. Further research is required how to apply this in balanced mechanisms.

5.3. Towards dynamically balanced multiple DoF mechanisms

The research in chapters 3 and 4 was focussed on the application to a single rotatable link. The rotatable link can be used as a building block in multiple DoF mechanisms. Figure 5.1 shows examples of force balanced 2 DoF mechanisms. Figure 5.2 shows examples of dynamically balanced mechanisms based on balanced inverted four-bar linkages. Both these figures show examples based on parallel architectures, which is based on the design principle from chapter 2, due to their higher stiffness and lower moving mass. In terms of controllability, it is beneficial to locate balancing elements close to the base and only balance proximate links. This is in correspondence with the design principle from chapter 2 that it is beneficial for settling time when mass of distal links is minimized. A dynamically balanced mechanism, with the balancing elements located at the base, can be achieved by basing the mechanism on a parallelogram of pantograph [5, 6, 16]. As this only requires to balance the proximate links, it will correspond with balancing a single rotatable link.

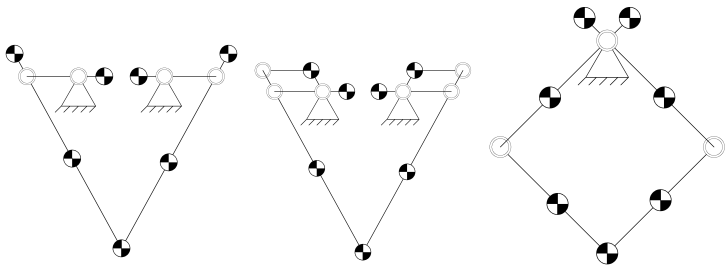

(a) Five-bar linkage with individual force balanced legs [1]

(b) Five-bar linkage with idler loops for force balancing (obtained by combination of two double pendulum which are balanced by using an idler loop [17])

(c) Force balanced degenerated five-bar linkage based on a pantograph [5]

Figure 5.1: Force balanced 2 DoF parallel architectures

As shown in Figure 5.1, shaking force balance for a 2 DoF mechanism can be achieved in multiple ways. Figure 5.1a individually balances each leg in the mechanism, although this approach results in more design freedom, controllability is limited [1]. Degeneration of natural frequencies in this architecture is, although it seems counter-intuitive, predominantly caused by the distal links. The extension of the distal links combined with the additional mass reduces natural frequencies significantly. Without adding kinematic relations it is possible to improve natural frequencies slightly by adding idler loops (Figure 5.1b). Removing the balancing masses from the distal links, with the help of a pantograph mechanism (Figure 5.1c), will result in significantly higher natural frequencies [5]. In addition, the moving mass and reduced inertia are lower. A pantograph is created when the proximate and distal links have equal length. Due to the kinematic relations when this condition is satisfied, balancing masses only have to be added to the proximate links [6].

A planar dynamically balanced 2 DoF parallel mechanism can be achieved with the architectures shown in Figure 5.2. The same considerations as with force balancing are applicable for dynamical balance. The architecture shown in Figure 5.2a will therefore, although it results in more design freedom, experience issues with the natural frequencies of the distal links. A pantograph based mechanism as shown in Figure 5.2b and 5.2c will result in significantly higher natural frequencies. Relocating the balancing elements of the distal links with idler loops is not possible due to the non-linear terms in the moment balance conditions. Figure 5.2c is a six-bar linkage based on a pantograph architecture. Additional requirements are, next to equal lengths of the distal and proximate links, that the base attached revolute joints need to be spaced at equal distance as the platform width (horizontal link attached at both proximate links). In addition, a mechanism needs to be added which fixes the platform horizontally [2, 4]. Main advantage of this architecture is more straightforward actuator placement and by spacing the base attached revolute joints results in higher stiffness.

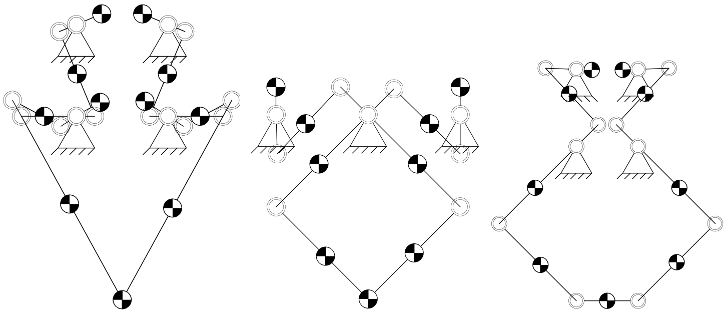

(a) Five-bar linkage with individual dynamically balanced legs (obtained by combination of two reactionless planar 2 DOF mechanisms [3])

(b) Proposed dynamically balanced degenerated five-bar linkage based on a pantograph

(c) Proposed dynamically balanced six-bar linkage based on a pantograph, rotation of the platform needs to be constrained (can be achieved with solutions proposed in [2] and [4])

Figure 5.2: Dynamic balanced 2 DoF parallel architectures

Creating complete dynamically balanced spatial mechanisms will be more challenging due to spatial kinematics and dynamics, which are difficult to balance. For a fully dynamically balanced manipulator is more research needed. Another solutions would be to only balance proximate links and accept that the mechanism is partially balanced. In this case the effect on settling time needs to be researched. The optimization and evaluation of performance of the proposed dynamically balanced planar 2 DoF mechanism architectures is an interesting topic for further research.

6 Conclusion

This thesis had the objective to investigate how settling time of robotic manipulators in a realistic mechatronic environment can be reduced with dynamic balancing. The literature study revealed that settling time is dependent on a variety variables. In addition, a multitude of solutions exist to improve settling time. As a general conclusion was found that a significant part of the settling time is determined by the controllability and acceleration capabilities of the mechanism. The controllability was found to depend significantly on the natural frequencies of the manipulator, therefore improving controllability requires to improve the stiffness and to reduce the moving mass and inertia of the mechanism.

Three principles to achieve dynamic balance were applied to a rotatable link and it was determined which principle has optimal controllability. In a comparison of frequency ratios it was shown that in the reference case an inverted four-bar linkage and separate counter-rotation (SCR) balancing have 6% higher frequency ratios than counter-rotating counter-mass (CRCM) balancing. When optimization of the link stiffness was allowed, the frequency ratio of counter-rotating CRCM-balancing increased with 14%, while SCR-balancing improved marginally. CRCM-balancing therefore outperforms SCR-balancing after optimization. Optimization of link stiffness in the balanced inverted four-bar linkage increased the frequency ratio with 63%. Based on these results the balanced inverted four-bar linkage showed significant higher potential to achieve high frequency ratios than SCR- or CRCM-balancing.

Based on the inverted four-bar linkage a novel dynamically balanced design was made with optimized controllability. The natural frequencies were theoretically verified in simulations to asses the performance of the final design. These simulations showed that the design had a first theoretical natural frequency of 312 Hz. The effect of manufacturing errors were investigated in simulations to determine the robustness of the design. A prototype was built for experimental verification. Chosen was to manufacture the prototype from tubes and laser cut sheet metal. This showed that a balanced mechanism can be produced with low cost production methods. An experimental setup was built, to suspend the base by chains, in order to determine the balance quality with load cells. Measurements showed a reduction in reaction forces of 99.3% and reaction moments of 97.8%, compared to the unbalanced mechanism. Robustness to tip mass deviations was experimentally verified with half of the tip mass, which can be regarded as near perfect balance. In this case a reduction in reaction forces of 90.3% and reaction moments of 81.9% was measured compared to the unbalanced mechanism. To evaluate the controllability a frequency sweep was conducted to determine the natural frequencies of the prototype. The first natural frequency of the prototype was 212 Hz. Acceleration capabilities were investigated, which ultimately lead to achieving transverse tip accelerations over 21 G. The experiments showed that high accelerations and controllability can be combined with dynamic balancing.

Architectures were presented how a balanced single rotatable link can efficiently be integrated in 2 DoF manipulators to achieve a dynamically balanced manipulator. With the research in this thesis a solid foundation has been laid for the design of dynamically balanced robotic manipulators in high acceleration applications to achieve low settling times.

Bibliography

[1] J J De Jong, B E M Schaars, and D M Brouwer. The influence of flexibility on the force balance quality: a frequency domain approach. *Proceedings of the 19th international conference of the European Society for Precision Engineering and Nanotechnology*, (June):2–5, 2019.

[2] Coralie Germain, Se´bastien Briot, Victor Glazunov, Ste´phane Caro, and Philippe Wenger. IRSBot-2: A Novel Two-DOF Parallel Robot for High-Speed Operations. In *Volume 6: 35th Mechanisms and Robotics Conference, Parts A and B*, pages 899–909. ASMEDC, jan 2011. ISBN 978-0-7918-5483-9. doi: 10.1115/DETC2011-47564.

[3] Clément M. Gosselin, Frank Vollmer, Gabriel Côté, and Yangnian Wu. Synthesis and design of reactionless three-degree-of-freedom parallel mechanisms. *IEEE Transactions on Robotics and Automation*, 20 (2):191–199, 2004. ISSN 1042296X. doi: 10.1109/TRA.2004.824696.

[4] Tian Huang, Zhanxian Li, Meng Li, Derek G. Chetwynd, and Clement M. Gosselin. Conceptual design and dimensional synthesis of a novel 2-DOF translational parallel robot for pick-and-place operations. *Journal of Mechanical Design, Transactions of the ASME*, 126(3):449–455, 2004. ISSN 10500472. doi: 10.1115/1.1711822.

[5] J.P. Karidis, G. McVicker, J.P. Pawletko, L.C. Zai, M. Goldowsky, R.E. Brown, and R.R. Comulada. The Hummingbird minipositioner-providing three-axis motion at 50 g's with low reactions. In *Proceedings 1992 IEEE International Conference on Robotics and Automation*, volume 1, pages 685–692. IEEE Comput. Soc. Press, 1992. ISBN 0-8186-2720-4. doi: 10.1109/ROBOT.1992.220288.

[6] Thierry Laliberté and Clément Gosselin. Synthesis, optimization and experimental validation of reactionless two-DOF parallel mechanisms using counter-mechanisms. *Meccanica*, 51(12):3211–3225, 2016. ISSN 15729648. doi: 10.1007/s11012-016-0582-0.

[7] Alberto Martini, Marco Troncossi, and Alessandro Rivola. Elastodynamic effects of mass-balancing: Experimental investigation of a four-bar linkage. *Advances in Mechanical Engineering*, 2013, 2013. ISSN 16878132. doi: 10.1155/2013/949457.

[8] Alberto Martini, Marco Troncossi, Marco Carricato, and Alessandro Rivola. Elastodynamic behavior of balanced closed-loop mechanisms: Numerical analysis of a four-bar linkage. *Meccanica*, 49(3):601–614, 2014. ISSN 00256455. doi: 10.1007/s11012-013-9815-7.

[9] J. P. Meijaard and V. van der Wijk. On the Dynamic Balance of a Planar Four-Bar Mechanism with a Flexible Coupler. In *Mechanisms and Machine Science*, volume 73, pages 3037–3046. 2019. ISBN 9783030201319. doi: 10.1007/978-3-030-20131-9_299.

[10] H. F. Menschaar, A. B. Ariens, J. L. Herder, and B. M. Bakker. Five-bar mechanism with dynamic balancing means and method for dynamically balancing a five-bar mechanism, 2006.

[11] Vincent Nabat, M. de la O Rodriguez, Olivier Company, Sébastien Krut, and F. Pierrot. Par4: very high speed parallel robot for pick-and-place. In *2005 IEEE/RSJ International Conference on Intelligent Robots and Systems*, pages 553–558. IEEE, 2005. ISBN 0-7803-8912-3. doi: 10.1109/IROS.2005.1545143.

[12] Shimon Y. Nof. *Handbook of industrial robotics*. Wiley, 1999.

[13] René Raaijmakers. Besi zoekt snelheidslimiet pakken en plaatsen op, Sep 2007. URL `https://mechatronicamachinebouw.nl/artikel/besi-zoekt-snelheidslimiet-pakken-en-plaatsen-op/`.

[14] Marc Teulieres, Jonathan Tilley, Lea Bolz, Peter Manuel Ludwig-Dehm, and Susanne Wägner. Industrial robotics: Insights into the sector's future growth dynamics, Jul 2019. URL `https://www.mckinsey.com/~/media/McKinsey/Industries/AdvancedElectronics/OurInsights/Growthdynamicsinindustrialrobotics/Industrial-robotics-Insights-into-the-sectors-future-growth-dynamics.ashx`.

[15] V. Van der Wijk, B. Demeulenaere, C. Gosselin, and J. L. Herder. Comparative Analysis for Low-Mass and Low-Inertia Dynamic Balancing of Mechanisms. *Journal of Mechanisms and Robotics*, 4(3):1–8, 2012. ISSN 19424302. doi: 10.1115/1.4006744.

[16] Volkert Van Der Wijk and Just L. Herder. Synthesis of dynamically balanced mechanisms by using counter-rotary countermass balanced double pendula. *Journal of Mechanical Design, Transactions of the ASME*, 131(11):1110031–1110038, 2009. ISSN 10500472. doi: 10.1115/1.3179150.

[17] Volkert van der Wijk, Just L. Herder, and Bram Demeulenaere. Comparison of various dynamic balancing principles regarding additional mass and additional inertia. *Journal of Mechanisms and Robotics*, 1(4): 1–9, 2009. ISSN 19424302. doi: 10.1115/1.3211022.

[18] Volkert van der Wijk, Sébastien Krut, François Pierrot, and Just L Herder. Design and experimental evaluation of a dynamically balanced redundant planar 4-RRR parallel manipulator. *The International Journal of Robotics Research*, 32(6):744–759, 2013. ISSN 0278-3649. doi: 10.1177/0278364913484183.

[19] M. J. Walker and R. S. Haines. An experimental study of the effects of counterweights on a six-bar chain. *Mechanism and Machine Theory*, 17(6):355–360, 1982. ISSN 0094114X. doi: 10.1016/0094-114X(82)90027-1.

[20] Yangnian Wu and Clément M. Gosselin. Synthesis of reactionless spatial 3-DoF and 6-DoF mechanisms without separate counter-rotations. *International Journal of Robotics Research*, 23(6):625–642, 2004. ISSN 02783649. doi: 10.1177/0278364904044400.

[21] Fengfeng Xi and Rosario Sinatra. Effect of dynamic balancing on four-bar linkage vibrations. *Mechanism and Machine Theory*, 32(6):715–728, aug 1997. ISSN 0094114X. doi: 10.1016/S0094-114X(97)83005-4.

A

Improvements in the experimental setup

The following improvements are suggested based on the experimental setup in chapter 4 for future experiments of balanced mechanisms:

- **Vibrations in the measurement setup**: This behaviour is also known as ringing, and is caused by the low stiffness of the load cells combined with fluctuating loads. Additionally, the connecting rods between the load cells and the base have limited transverse stiffness. The low stiffness of both elements resulted in a rotational vibration of the base with a frequency of 18.18 Hz. Solving this issue would require stiffer load cells. Stiffer load cells will deflect less at equal force, therefore the transverse stiffness of the connection rods between the load cells and base could be increased without disturbing measurements.
- **Measurement triggering**: The measurements were recorded separately from the motions, therefore it was required to manually match measurements. Triggering the measurement when the motion starts will make measurements and motion match without post-processing.
- **Reduced natural frequencies due to base elasticity**: The base, to which link 1 and 3 are attached, has limited stiffness in the experimental setup. The natural frequencies are therefore limited by the base, increasing the stiffness with a more rigid design would result in higher natural frequencies.
- **Feedforward control**: Addition of feed-forward means the feedback control can be tuned for disturbance rejection instead of tracking. The result of this improvement is that less actuation torque is used for accelerations compared to feedback control only. Higher accelerations are therefore achievable before actuator saturation. Main challenge in implementing feedfoward control is that a computer with a real time operation system is required to calculate actuation torques real time.
- **Monolithic links**: The links in the experiment are based on tubes and laser cut plates. The tubes have tolerances in their straightness and squareness, which cause deviations in the mass distribution. The result is that the balance quality becomes lower. To solve this issue monolithic links need to be milled with a CNC mill.
- **Extension of suspension chains**: Increasing the length of the suspension chains allows the larger horizontal movements of the subframe without moving vertically. This will result in more precise measurements, because part of the reaction force is not used to move the base vertically. Even better results could be achieved by changing to a setup based on air or ferro fluid bearings.